

Modeling Day-Long ECG Signals to Predict Heart Failure Risk with Explainable AI

Eran Zvuloni^{1*}, Ronit Almog^{1,2}, Michael Glikson³, Shany Brimer Biton¹, Ilan Green⁴,
Izhar Laufer⁴, Offer Amir⁵, Joachim A. Behar^{1*}

¹Faculty of Biomedical Engineering, Technion-IIT, Haifa, Israel.

²Epidemiology Unit, Rambam Health Care Campus, Haifa, Israel.

³Jesselson Integrated Heart Center, The Eisenberg R&D Authority, Shaare Zedek Medical Center, Faculty of Medicine, Hebrew University, Jerusalem, Israel.

⁴Leumit Health Services, Tel Aviv-Yafo, Israel.

⁵Heart Institute, Hadassah Medical Center, Faculty of Medicine, Hebrew University, Jerusalem, Israel.

*Corresponding author(s). E-mail(s): eranzvuloni@gmail.com; jbehar@technion.ac.il;

Abstract

Heart failure (HF) affects 11.8% of adults aged 65 and older, reducing quality of life and longevity. Preventing HF can reduce morbidity and mortality. We hypothesized that artificial intelligence (AI) applied to 24-hour single-lead electrocardiogram (ECG) data could predict the risk of HF within five years. To research this, the Technion-Leumit Holter ECG (TLHE) dataset, including 69,663 recordings from 47,729 patients, collected over 20 years was used. Our deep learning model, DeepHHF, trained on 24-hour ECG recordings, achieved an area under the receiver operating characteristic curve of 0.80 that outperformed a model using 30-second segments and a clinical score. High-risk individuals identified by DeepHHF had a two-fold chance of hospitalization or death incidents. Explainability analysis showed DeepHHF focused on arrhythmias and heart abnormalities, with key attention between 8 AM and 3 PM. This study highlights the feasibility of deep learning to model 24-hour continuous ECG data, capturing paroxysmal events and circadian variations essential for reliable risk prediction. Artificial intelligence applied to single-lead Holter ECG is non-invasive, inexpensive, and widely accessible, making it a promising tool for HF risk prediction.

Keywords: Heart failure, deep learning, Holter, electrophysiology, circadian, raw physiological time series

Heart failure (HF) is a complex, generally chronic syndrome, characterized by a wide range of symptoms that can interfere with daily activities and carries significant morbidity and mortality implications [1–3]. HF is marked by a continuous abnormal cardiac function and/or structure [1], along with clinical manifestations of elevated filling pressures and/or reduced cardiac output. Risk factors include among others coronary artery disease, arrhythmias, hypertension, cardiac toxins such as alcohol, valvular heart disease, infiltrative and inflammatory diseases, and specific genetic mutations [3]. Its clinical severity may be classified based on functional status, such as the New York Heart Association (NYHA) classification, six-minute walk tests and cardiopulmonary exercise tests [3, 4]. HF is traditionally categorized according to the ejection fraction (EF), which is usually measured by echocardiography, as preserved (HFpEF), mildly reduced (HFmrEF) or reduced (HFrEF). A more recent four-stage (A-D) classification, introduced by the American College of Cardiology/American Heart Association (ACC/AHA), focuses on the continuum of disease, from risk factors to advanced HF [5].

Globally, HF affects approximately 64 million people [1], with a prevalence of 1-2% among adults in developed countries and approximately 11.8% in adults over 65 [1]. The increasing average age of the population and longer life expectancy have contributed to the increasing incidence of HF [6], which is now a leading cause of hospitalization in adults over 60 years [2]. HF progresses over several years, resulting in a gradual decline in quality of life and increased mortality [3]. The differential diagnosis of HF can be challenging due to the overlap of symptoms of comorbidities such as renal failure, chronic obstructive pulmonary disease and liver disease. The AHA emphasizes that early management of risk factors can prevent or slow HF progression, and advocates timely detection and prevention strategies [3, 7]. Indeed, early detection of HF has been associated with reduced mortality, improved quality of life and decreased economic burden on the health system [3].

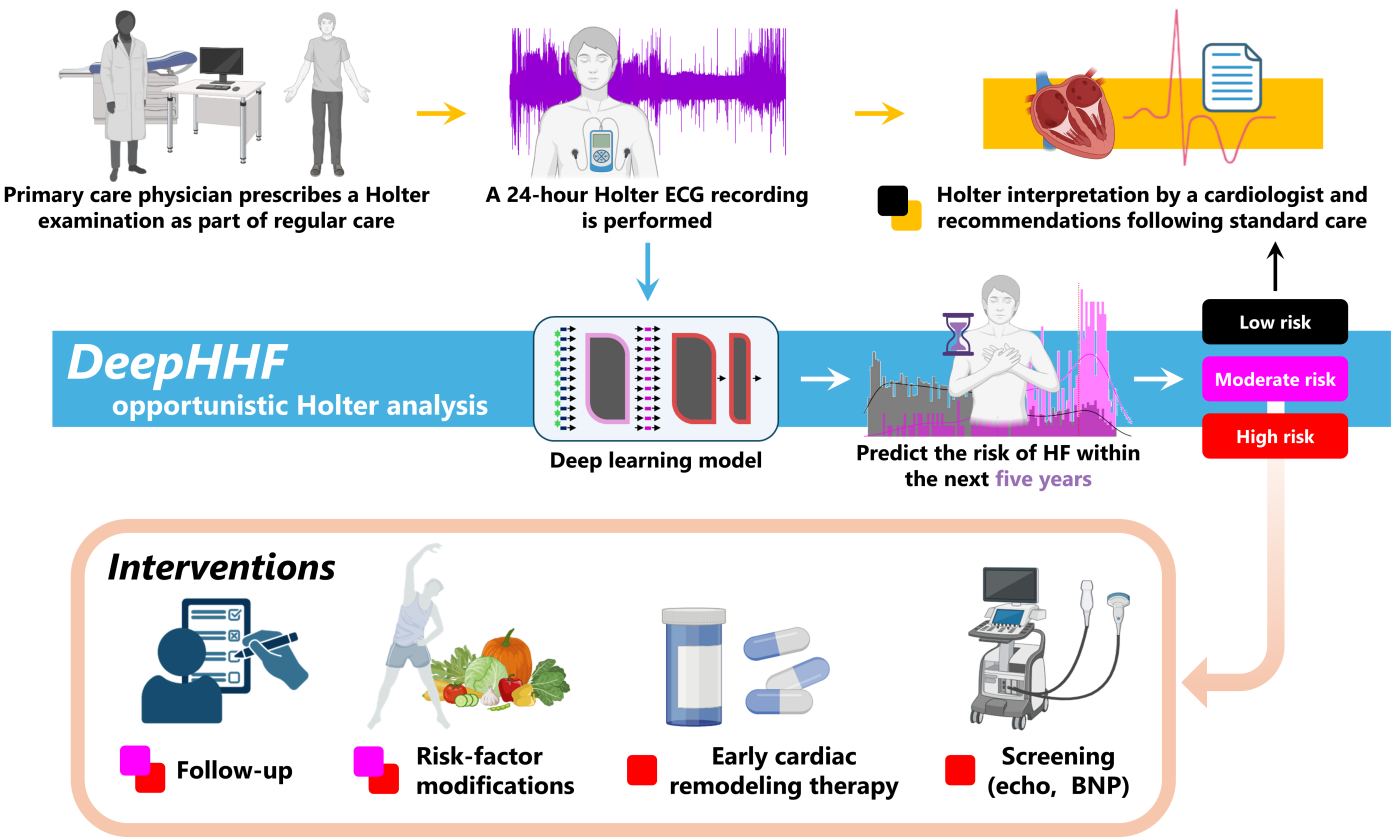


Fig. 1: Perspective clinical scenario for using the DeepHFF score. The patient undergoes a Holter ECG examination for regular indications, such as suspected arrhythmia or syncope. The ECG recording is then processed as an opportunistic analysis by the DeepHFF model and outputs a heart failure (HF) risk score. Patients identified as being at moderate or high risk could be directed toward preventive actions, such as additional screening with brain-type natriuretic peptide (BNP) testing or echocardiography. The icons were created with BioRender.com.

Artificial intelligence (AI), particularly deep learning (DL) algorithms, has become a powerful tool for uncovering complex patterns in data, and surpasses the limitations of traditional engineered features designed based on the data, which are constrained by human assumptions. DL has already been successfully applied for electrocardiogram (ECG) analysis, with various applications, such as arrhythmia diagnosis [8], atrial fibrillation risk prediction [9], occlusion myocardial infarction detection [10], and identifying chronic diseases such as kidney disease [11]. DL-based ECG research has focused mainly on 12-lead ECG analysis, which provides a snapshot of the patient's physiological state over a short period, typically around 10 seconds. Although standardized and commonly used in medical practice, the 12-lead ECG can miss paroxysmal events and circadian variations that could be captured by Holter ECG, which records ECG for 24 hours or more. In the context of HF, DL based on 12-lead ECG has been used to identify individuals with an EF $\leq 35\%$ [12, 13], a condition often associated with HF. Despite this seminal study, the approach of identifying low EF is inherently focused on patients with HFrEF, and therefore would miss approximately half of cases of HF that are HFmrEF or HFpEF [14, 15].

Since cardiovascular risk factors for HF are associated with cardiovascular conditions that can affect the heart's electrical conduction system, leading to changes in the ECG [16], identifying these patterns may enable the early detection of individuals at risk of future HF. Consequently, we hypothesized that AI applied to single-lead 24-hour ECG data can predict the risk of developing HF within five years. To test this hypothesis, we developed a large database of Holter ECG and associated 20-year-long clinical data. This work presents Deep Holter Heart Failure (DeepHFF), a DL model for 5-year HF risk prediction. Its output score can be obtained during primary care cardiac examinations and is expected to opportunistically aid in identifying high-risk individuals, thereby enabling their prioritization for periodic follow-up and interventions (Figure 1).

Results

The main objective of this work was to develop a model capable of predicting HF risk from a single-lead ECG Holter examination performed in a primary care setting. To achieve this, the Technion-Leumit Holter ECG (TLHE) dataset was developed. The dataset included Holter ECG recordings coupled with comprehensive time-stamped demographic data, diagnoses, admissions, visits, lab results, measurements, treatments, and medications. The HF endpoint was established by extracting the first documented HF diagnosis per patient. Holter recordings within five years prior to the endpoint were considered to belong to the positive class (HF). All other recordings constituted the negative class (non-HF). A total of

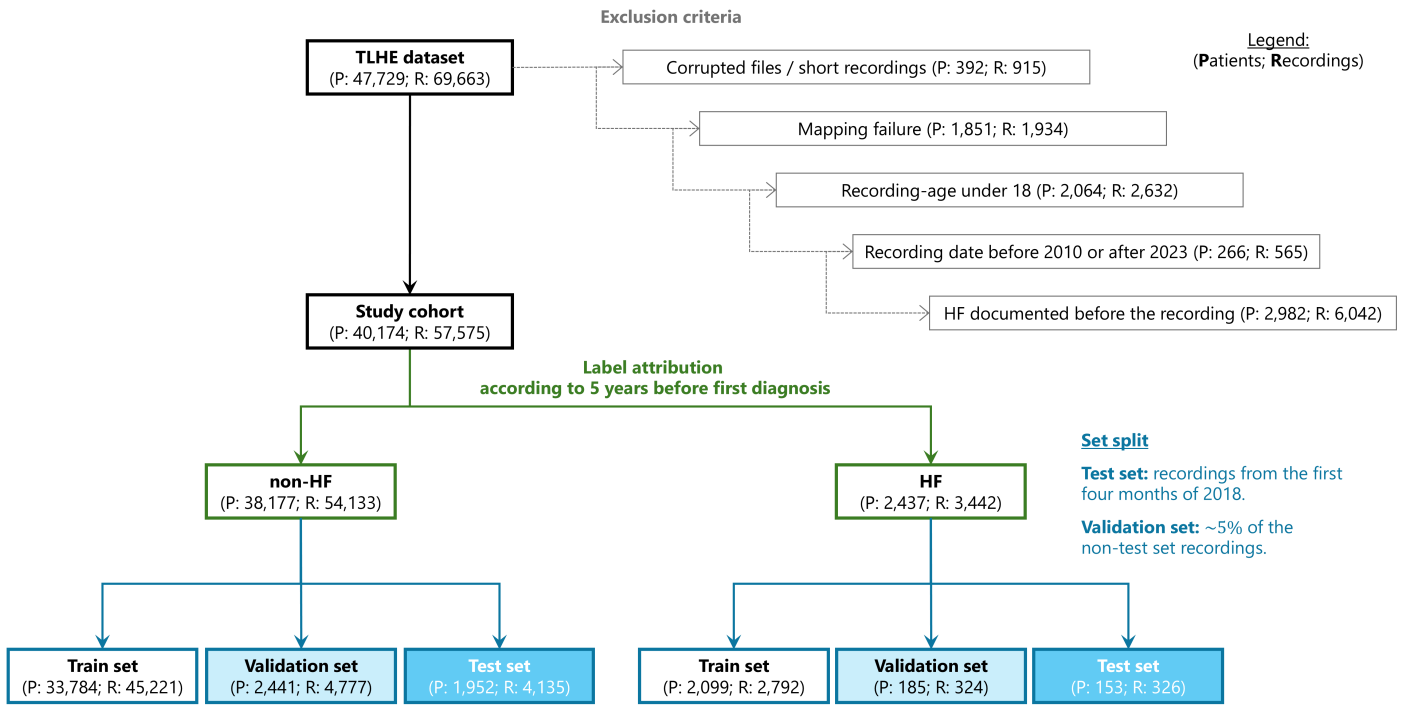


Fig. 2: Cohort definition and experimental settings. The flow diagram shows patient inclusion and exclusion criteria, the definition of the two classes with respect to heart failure diagnosis (HF) or lack thereof (non-HF) within five years of the Holter ECG recording, and the partition between training and test sets.

6,042 Holter examinations with a documented prior diagnosis of HF were excluded from the study cohort (Figure 2). A DL model, denoted DeepHHF, was trained in two steps. First, an encoder was trained to extract features from independent 30-second windows of single-lead 24-hour Holter recordings. Second, features of the pre-trained encoder were fed into a sequential head that accounted for the sequential nature of the 24-hour long recording. In this way, following analysis of the entire 24-hour ECG recording, DeepHHF produced a score for probability of developing HF within 5 years.

Study cohort characteristics

The TLHE dataset includes 69,663 Holter recordings from 47,729 unique patients collected from 20 primary care facilities in Israel, along with 20 years of clinical data. After applying exclusion criteria (Figure 2), and excluding recordings that had HF diagnosis documented prior to Holter examination, the study cohort consisted of 57,575 Holter ECG recordings from 40,174 unique patients, with 10,037 patients (25.0%) having more than one Holter recording. The median age at the recording time was 63 years (interquartile: 48–72) and 6.0% of the recordings had an incident HF endpoint documented within 5 years of Holter examination. A total of 59.8% of the patients were women. Furthermore, 26.2% of the patients had a documented cardiac dysrhythmia before the recording time, 23.3% had diabetes, 49.9% had hypertension, and 25.4% had ischemic heart disease (including myocardial infarction and acute coronary events). To prepare the study cohort data for the DL pipeline, the recordings were divided into a training set and a test set. Specifically, the test set was defined to include all consecutive Holter recordings from the first four months of 2018, ensuring that all test set patients had a complete 5-year follow-up period. A patient-specific stratification was applied to prevent possible information leakage between sets. The characteristics of the cohort are presented in Table 1.

Deep learning

Figure 3a shows the results obtained for the DL encoder model trained on 30-second window and DeepHHF which was trained on the entire 24-hour-long recording. When training on individual 30-second windows, the DL model yielded an area under the receiver operating characteristic curve (AUROC) of 0.77. When adding the sequential transformer head to the trained encoder in order to train the model over the full 24-hour recording, DeepHHF achieved AUROC=0.80. When separating between recordings belonging to male and female patients, AUROC remained 0.80 for both groups. The performance of the DeepHHF model was compared with that of the PCP-HF score [17] for HF risk prediction, as recommended by the 2022 AHA/ACC/HFSA guidelines [3]. The PCP-HF score classification performance had an AUROC=0.74 (Figure 3b), which was significantly (p -value < 0.05) lower than the DeepHHF AUROC. All performance reported are for the test set.

To evaluate whether incorporating demographic and comorbidity history variables from the TLHE dataset could improve model performance, these were combined with the DeepHHF score as input to a logistic regression classifier. Incorporating the patient variables listed in Table 1 resulted in an AUROC of 0.82 (Extended Data Figure 7a). Similarly,

augmenting the DeepHHF score with the variables used to compute the PCP-HF score also yielded an AUROC of 0.82 (Extended Data Figure 7b).

Error analysis

When evaluating DeepHHF performance according to subgroups defined by the time interval between Holter examination and the first documented HF diagnosis (Figure 4a), the model demonstrated consistent performance with an AUROC=0.81, for examinations performed within two years prior to the first documented HF diagnosis. Performance declined to AUROC=0.79 for examinations conducted 2-4 years prior to the first documented HF diagnosis. A further performance decrease to AUROC=0.77 was observed for recordings taken 4-5 years prior to the first documented HF diagnosis. In a second analysis, Kaplan-Meier survival curves were produced for both all-cause mortality and either cardiac/internal department hospitalization or all-cause mortality (Figure 4b). An 90% specificity threshold, defined as the decision boundary separating between the high-risk group versus the low/moderate-risk groups in Figure 3c, was used to generate the curves for the false positive (FP), true negative (TN), true positive (TP), and false negative (FN) groups in the test set. The TP, FP and FN groups exhibited significantly lower (p -value < 0.05) survival rates than the TN group. Furthermore, the TP, FP and FN groups exhibited a higher proportion of comorbidities associated with HF compared to the TN group (Figure 4c). Of particular mention, the findings highlighted that while the FP group had no documented HF within five years of Holter examinations, the patients were in poor cardiovascular health. This is reflected by the low survival, similar to the TP group (Figure 4b), as well as the cardiovascular comorbidities (Figure 4c) with prevalence very similar to those in the TP group. In contrast, patients in the TN group had a much lower proportion of these comorbidities and had better survival rate than patients in the TP and FP groups.

Clinical value

Figure 3c presents the distribution of the class (HF or non-HF) prediction by the DeepHHF model. Low, moderate, and high-risk groups were defined based on probability thresholds. A specificity of 70% was used to distinguish low-risk from non-low-risk groups, while a specificity of 90% was applied to separate non-high-risk from high-risk groups. The lower panels in Figure 4b show the Kaplan-Meier curves for the low, moderate and high risk groups. The TP and FP groups had the same survival trajectory, which emphasized that all individuals identified by the model as high-risk indeed had low survival. A comparison between the encoder part of the model based on 30-second recording inputs (dashed lines), versus the full DeepHHF model based on the whole 24-hour recording as input (solid lines) was made. The DeepHHF separated the different risk groups better, distinguishing more between patient who are prone to death and hospitalization incidents. Additionally, odds ratios were calculated to compare between the two groups, yielding an odds ratio of four for mortality and two for hospitalization or death. This indicates that individuals in the high-risk group are four times more likely to experience death and twice more likely to experience either hospitalization or death compared to those in the low/moderate-risk group.

Model explainability

Explainability analysis was conducted in order to provide insights on how DeepHHF makes its decisions. Figure 5a shows an example of a 24-hour ECG recording from the positive class. The green curve highlights time intervals with high model attention. Figure 5b shows the attention intensity with respect to day time for all HF test set recordings. Figure 5c shows the average attention intensity with respect to day time. When considering 99% of the attention, it was concentrated within the 7 AM - 8 PM interval, and when considering 95% of the attention, the peak attention was between 8 AM and 3 PM. When using unsupervised learning to cluster heartbeats with a high level of attention, four clusters were discovered. Figure 5d shows averaged beats reflecting these four clusters. The morphology of these averaged beats resembled: 1) premature ventricular contraction with two clusters displayed in yellow and gray; 2) normal sinus rhythm with one cluster displayed in green; and 3) supraventricular ectopy with a narrow QRS and no P-wave displayed in pink.

External Validation

DeepHHF was further evaluated on an external cohort from Rambam Health Care Campus (Haifa, Israel), consisting of 150 Holter examinations from unique patients without a HF diagnosis at baseline. Of these, 29 patients were diagnosed with HF within the following three years. DeepHHF was applied to these recordings in a zero-shot setting (i.e., no fine-tuning), achieving an AUROC of 0.81. This analysis supports the validity of the model in a broader, more generalizable context.

Discussion

The main contribution of this research lies in the modeling of continuous 24-hour ECG recordings for HF risk prediction. To our knowledge, no previous work has explored the feasibility of predicting the risk of HF at 5-year from raw ECG data. Furthermore, although earlier studies have developed DL models using 12-lead ECG as input for risk prediction tasks [9, 20–22], none have used 24-hour raw ECG recordings for such tasks. Using the full 24-hour data, it is possible to

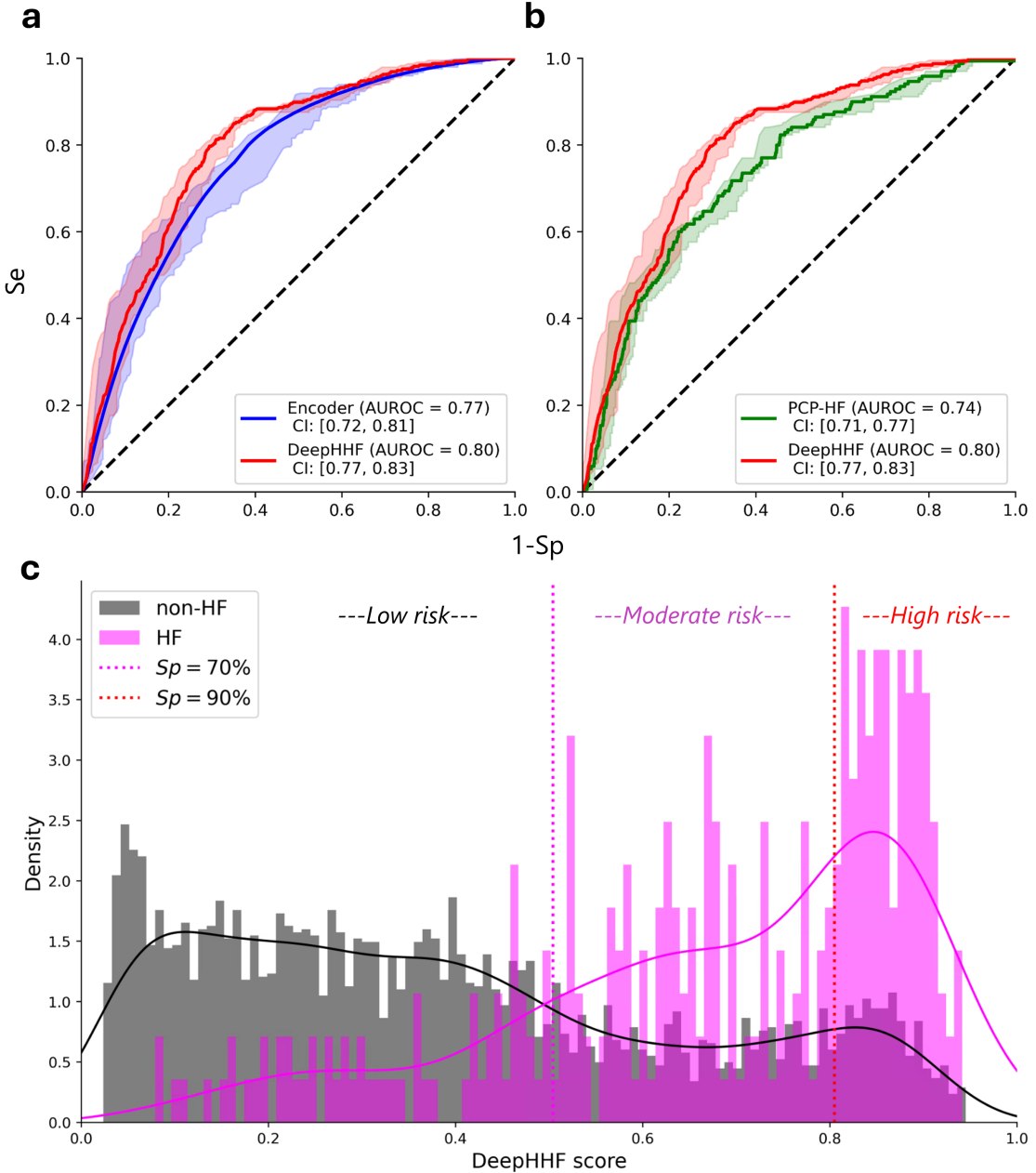


Fig. 3: Models' performance. Receiver operating characteristic curves (ROC) were produced for the test set. The area under ROC (AUROC) scores are provided with 95% confidence intervals (CI), shown as shaded area and evaluated by bootstrapping the test set. **a**, DeepHHF taking as input the 24-hour single ECG recording (red) vs. the encoder model taking as input a single 30-second ECG window (blue). **b**, DeepHHF vs. the PCP-HF clinical score [17] (green). The PCP-HF ROC curve is produced based on 1,917 test set examinations for which all the PCP-HF necessary variables were available (see Methods section). **c**, DeepHHF probability output distribution, separating the non-HF (gray) and HF (purple) classes. Sub-groups were divided into low-, moderate- and high-risk for HF according to the model probability risk scores. The moderate- and high-risk groups were defined by a probability decision threshold corresponding to Sp of 70% and 90%, respectively.

capture temporal task-associated patterns that may be missed in shorter ECG recordings, and may improve prediction performance.

The 2022 AHA/ACC/HFSA guidelines [3] recommended the use of risk scores to screen patients at high risk of developing HF. Among these, PCP-HF [17] (2019) was highlighted as the most recent score, allowing evaluation of patient risk for HF over a 10-year period, with performance ranging from 0.74 to 0.87 [17] and 0.69 to 0.84 [23] in race- and sex-specific models. Although DeepHHF was found to perform significantly (p -value < 0.05) better (AUROC=0.80) than PCP-HF (AUROC=0.74) on this research test set, it is important to note that the PCP-HF score was originally developed to predict the risk of HF among people aged 30–79 years without a history of cardiovascular disease. Alternative risk prediction scores for HF exist for groups with a cardiovascular history [24], but have shown modest performance.

DL analysis of ECG records has previously shown promise for HF detection. Attia et al. [12, 13] developed a model using 12-lead ECG data to identify systolic cardiac dysfunction ($EF \leq 35\%$). Their model achieved AUROC scores of

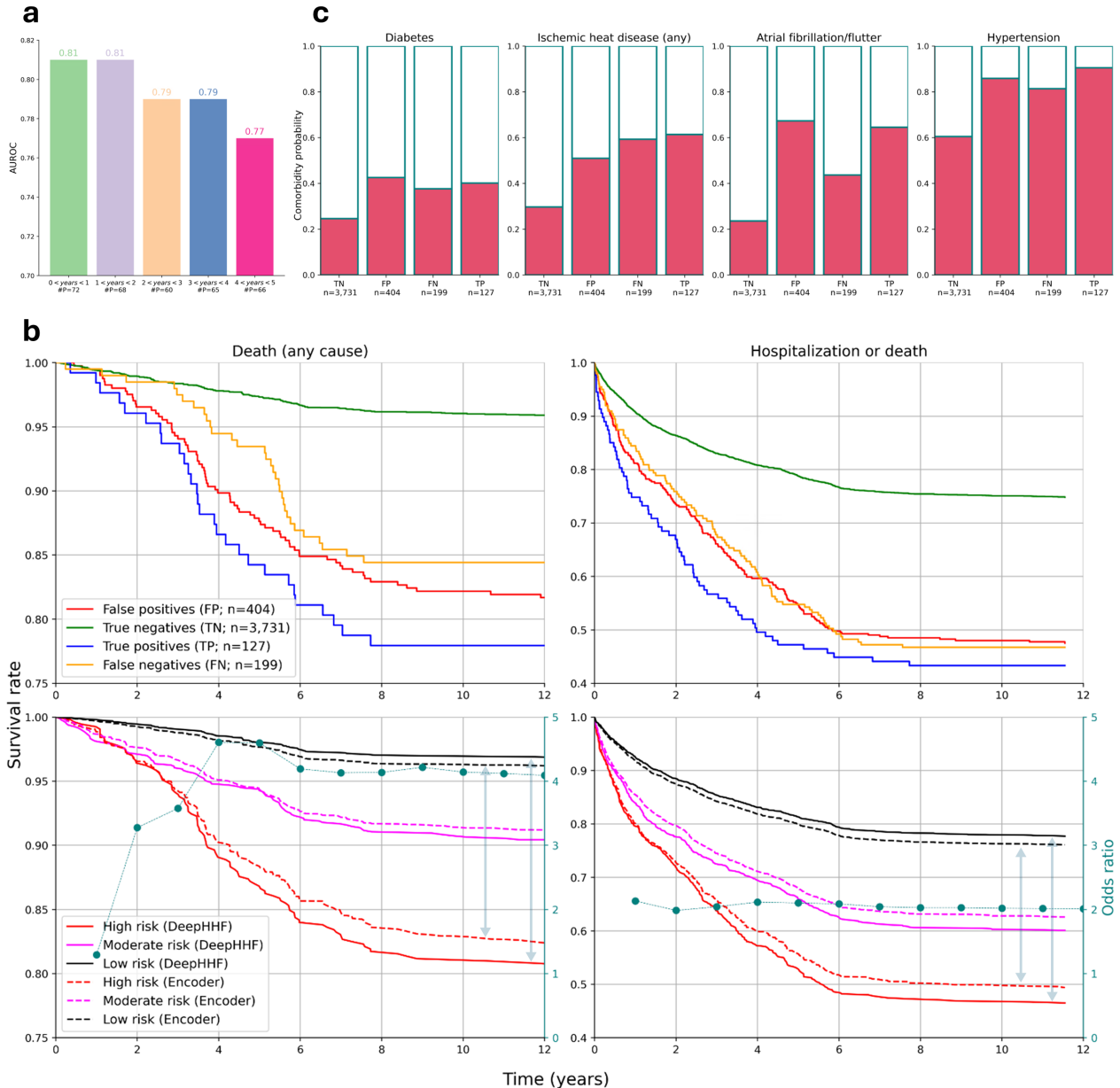


Fig. 4: Error analysis and clinical value of the DeepHHF model. The analysis is reported for the test set. **a**, Model performance for subgroups according to the time interval between the recording date and the first documented diagnosis of HF. Area under receiver operating characteristic curves (AUROC) are shown for each subgroup. $\#P$ is the number of positive examples contained in each interval. **b**, Kaplan-Meier analysis for death of any cause (left panels) and cardiac/internal department hospitalization or death of any cause (right panels). Upper panels show the Kaplan-Meier curves for the FP, TN, TP and FN groups. Lower panels show the Kaplan-Meier curves for the low, moderate and high risk groups as identified by the encoder (30-second window input) and by the DeepHHF model (full 24-hour recording input). The arrows illustrate the performance gap difference between using the short and long recordings. The odds ratio between the high and low/moderate survival curves are shown in the right y-axis (teal). **c**, Prevalence of known HF risk factors in the false positive (FP), true negative (TN), true positive (TP), and false negative (FN) groups, based on data available prior to the first HF diagnosis.

0.93 on a retrospective cohort [12] and 0.91 on a prospective cohort [13]. Despite this seminal research, the model was intended to detect HF prevalence rather than to predict the risk of new HF occurrences. Furthermore, the approach, which focuses on EF estimation and identifies only individuals with low EF, defined in their work as less than 35%, inherently would overlooks nearly half of HF patients with either mildly reduced or preserved EF; HFmrEF and HFpEF respectively. On the contrary, our study addresses this unmet clinical need by identifying patients at risk for HF across the entire spectrum of EF subtypes. Additionally, several recently published AI-ECG models have demonstrated the ability of 12-lead short-term ECG recordings to predict future HF occurrences. Some of these models relied on raw voltage time-series data, while others used image-based representations of ECG printouts. When extracting information solely from the ECG data, Dhingra et al [25] reported C-statistics ranging from 0.72 to 0.81 in three multinational cohorts. Similarly, Butler et al. [26] achieved an AUROC of 0.77 for predicting 10-year HF risk, and Akbilgic et al. [27] reported an AUROC

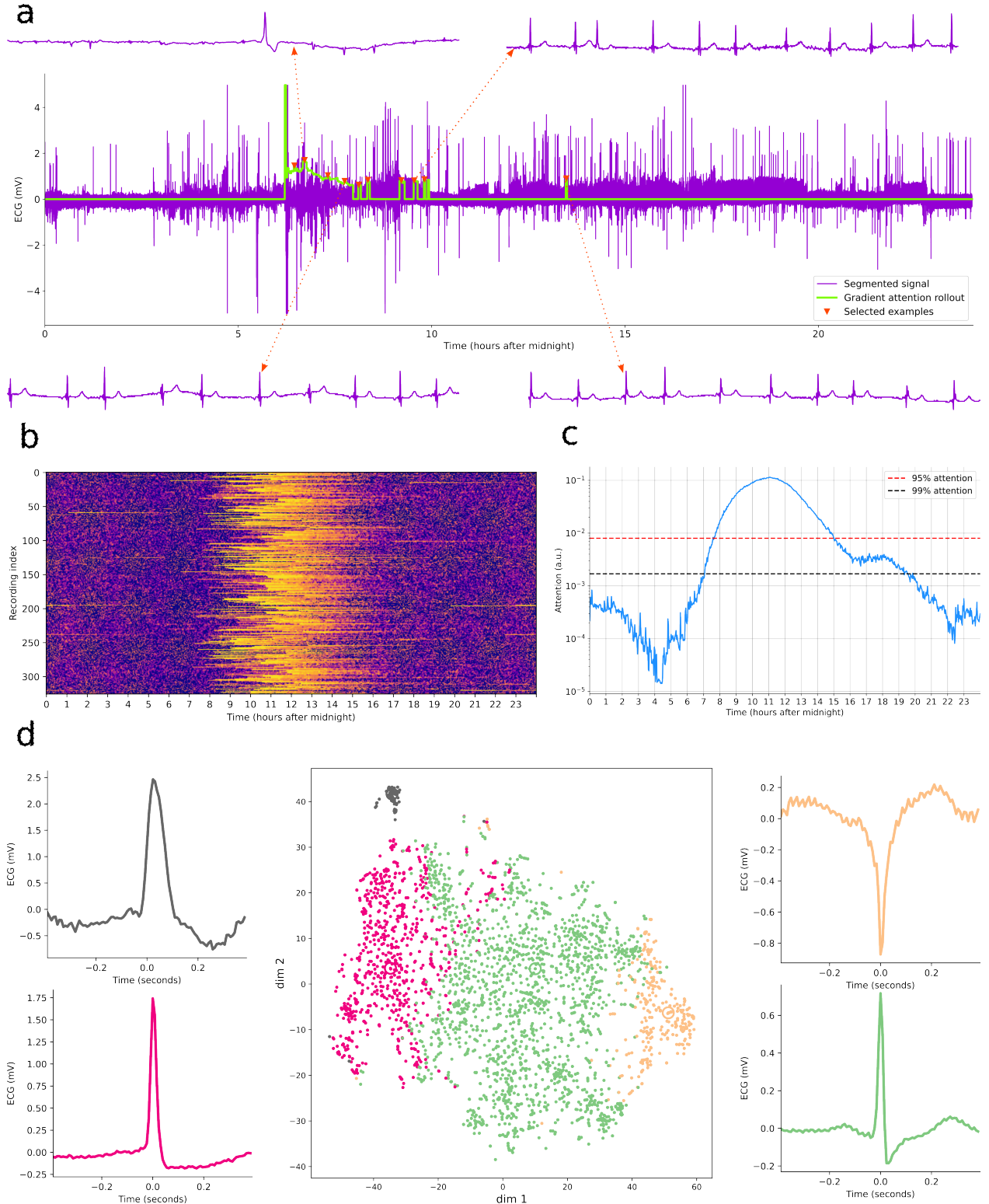


Fig. 5: DeepHHF model explainability analysis. The analysis was performed with the gradient attention rollout method [18, 19]. **a**, A single 24-hour recording example (purple) and associated gradient attention rollout map (green). The intervals with high attention were sampled (red triangles) for characteristic beat extraction. Four examples of 10-second ECG segments in regions of high attention are shown. **b**, Visualization of the gradient attention rollout maps displayed for all test set HF recordings ($n=326$). High attention is displayed in yellow (log-scale). **c**, Circadian variability analysis performed by averaging gradient attention rollout masks accumulated for the non-HF and HF test set recordings. **d**, **Middle panel:** t-SNE visualization for the k-means clustering, applied on the beats extracted from HF-class recording. Each point in the graph corresponds to a single beat, with reduced dimensions by t-SNE from 100 ECG samples ($\sim 0.78ms$) into 2 dimensions (dim 1, dim 2). The colors represent the four clusters found. **Side panels:** The beats from each cluster were averaged, obtaining characteristic beats for each cluster.

of 0.76 in the ARIC study cohort. In contrast, DeepHHF leverages long-term single-lead Holter recordings and achieves an AUROC of 0.80, which is comparable or exceeds previously reported performances. However, those studies [25–27] were conducted in cohorts where HF was defined primarily by hospitalization events, whereas DeepHHF was evaluated using a broader definition of HF onset, largely captured through primary care diagnoses.

A number of research studies have focused on risk prediction tasks for cardiovascular and systemic diseases from the ECG [9, 20–22]. The studies used short 12-lead ECG recordings, typically about 10-second. From an engineering perspective, the modeling of 24-hour raw ECG data performed here is a much more complex undertaking due to the challenges of handling such large volumes of raw data and capturing the sequential information embedded in the recordings. Use of the full 24-hour ECG signal compared to a 30-second ECG window resulted in a significant improvement in AUROC, from 0.77 to 0.80 (Figure 3a). This suggesting that there is considerable value in modeling the ECG dynamic over long recordings, as it enables the capture of time-dependent patterns associated with the endpoint. This is coherent with the fact that some arrhythmias, such as atrial fibrillation or the occurrence of ectopic beats, are paroxysmal in nature, and longer recordings may be necessary to detect them and assess their intensity or burden. Works in other fields of physiological time-series analysis, for example the task of sleep staging from polysomnography data [28], have demonstrated the benefits of using encoder–predictor style architectures to handle long-term recordings. Nevertheless, these approaches typically operate in a many-to-many fashion, in which each epoch in the signal is classified separately, rather than encoding the entire recording into a single prediction in a many-to-one fashion, as performed in this study.

The performance of the model was highest for people diagnosed with HF within two years of Holter examination (AUROC of 0.81, Figure 1a), compared to those diagnosed 3–5 years later (AUROC between 0.79 and 0.77). This result was expected, as imminent HF is likely associated with a greater presence or increased burden of cardiac abnormalities and arrhythmias. In contrast, HF prediction several years before onset is more challenging, as it requires the model to detect more subtle changes in the ECG, while also adjusting for variability introduced by factors such as lifestyle changes and medical interventions. In addition, patients newly diagnosed with HF may be recorded in the electronic medical record (EMR) of the health maintenance organization (HMO) several months after their initial diagnosis. Consequently, undiagnosed prevalent HF cases with active symptoms and treatments at the time of Holter recording could influence the ECG data and potentially inflate model performance. For this reason, it was important to observe that the performance of the model remained consistent within the first two years, as shown in Figure 1a. This shows the ability of the model to predict the risk of HF even in patients whose diagnosis was documented more than a year after their Holter examination. In addition, the TLHE dataset includes three ECG leads per Holter recording. Although our research focused on single-lead ECG modeling, aligned with the development of modern ECG patch technologies, we conducted several experiments during model development using all three leads as a three-channel input. However, these experiments did not show any improvement over the single-lead approach. Future research may better leverage multi-lead information through alternative modeling strategies.

The error analysis showed that specific comorbidities are associated with the FP group (Figure 4c). Specifically, comorbidites that are known risk factors for the development of HF [3], including hypertension, diabetes, ischemic heart disease and cardiac dysrhythmia, were observed to be highly prevalent in the FP group and in a proportion similar to that of the TP group, while having higher rates compared to the TN group. This observation suggests that DeepHHF is capable of learning subtle patterns in the ECG that are associated with cardiac electrical abnormalities as well as metabolic disorders and kidney failure (Extended Data Figure 1). The similarity between the survival curve trajectories of the FP and TP groups (Figure 4b) highlights some model’s additional non HF-specific clinical value as well.

DeepHHF has significant clinical value in identifying patients at high risk for HF. Our findings indicate that patients identified as high-risk had a forthcoming fourfold increased likelihood of all-cause mortality compared to low/moderate-risk patients. Similarly, high-risk patients had a forthcoming twofold increased likelihood of either all-cause death or cardiac/internal department hospitalization (Figure 4b). A recent randomized clinical trial [29] demonstrated that using AI-ECG to identify patients with a high-risk of mortality can enable timely clinical interventions and reduce mortality. DeepHHF can also be applied to select high-risk populations in clinical trials focused on HF prevention. Since DeepHHF requires only a single-lead ECG without additional clinical variables, it can easily be integrated into standard Holter analysis software or utilized in modern ECG devices such as single-lead ECG patches.

The explainability analysis was based on the gradient attention rollout method [18, 19]. While traditional raw attention weights have been criticized for lacking causal grounding [30], this limitation was addressed by combining attention weights with gradient information to more accurately trace the influence of inputs on the model’s output. This approach has been shown to achieve better alignment with attribution methods based on input gradients and to provide more reliable explanations [31, 32]. By incorporating gradients directly into the explainability maps, concerns associated with purely visualizing raw attention are mitigated. The explainability analysis (Figure 5c) highlighted that the majority of the model’s attention was within the time interval 7AM–8PM (99% of the model attention) and with a peak within 8AM–3PM (95% of the model attention), which is consistent with the circadian-onset patterns of arrhythmia that are mostly reported during daytime [33]. For example, premature atrial beats have their main peak incidence at 6AM–12PM, ventricular premature beats at 6AM–12PM adrenergically mediated atrial fibrillation at 6AM–12PM and ventricular tachycardia at 10AM–6PM. Those previous reports strengthen our interpretation that the DL model learns end-to-end to recognize patterns characteristic of arrhythmias that are associated with the development of HF. However, the attention energy may also reflect other physiological or behavioral factors. These include increased variability in heart rate due

to physical activity, autonomic fluctuations, or heart rate recovery dynamics, all of which tend to be more pronounced during waking hours. Thus, while circadian influence is a plausible contributor, the observed attention pattern likely reflects a combination of time-dependent physiological processes and is possibly related to HF as well. The averaged beat analysis (Figure 5d), based on the HF recordings, identified four types of characteristic ECG beats associated with the development of HF. In particular, abnormal beat morphologies were identified that resemble premature ventricular contractions (two clusters in yellow and gray) and supraventricular ectopic beats (in pink). These morphologies indicate the presence of ectopic beats, which are known to be associated with HF development [34]. Furthermore, absent P waves were observed, a feature known to be associated with atrial fibrillation, which is a common comorbidity of HF [35, 36].

To evaluate the potential value of DeepHHF in improving clinical outcomes, we sought quantitative evidence on the effectiveness of preventive strategies in individuals at high-risk for developing HF. The STOP-HF randomized control trial [37] assessing the impact of brain-type natriuretic peptide (BNP) screening followed by HF prevention strategies demonstrated that the interventions implemented in individuals with elevated BNP levels (≥ 50 pg/mL) effectively reduced emergency hospitalizations for major cardiovascular events (MACE), from an incidence rate ratio (IRR) of 0.60. However, in an editorial accompanying the trial results, Hernandez et al. [38] raised concerns about the feasibility of widespread BNP screening, and highlighted the need for targeted approaches to identify high-risk patients. Our findings show that DeepHHF improves the identification of moderate- and high-risk groups, thereby enabling reductions in both the number of patients requiring BNP screening and the number needed to screen (NNS) in order to prevent MACE hospitalizations. Specifically, when applying the settings from the STOP-HF trial [37], we observed MACE hospitalization incidence rates of 41.5 (compared with 40.4 reported by STOP-HF), 85.0, and 124.0 per 1,000 patient-years for the entire test set, moderate-risk subgroup, and high-risk subgroup, respectively. The corresponding NNSs were 61, 30, and 21, suggesting that DeepHHF significantly reduces the NNS. These results highlight the model's potential to prioritize high-risk patients for preventive HF interventions. Additionally, when comparing the performance of DeepHHF using 24-hour Holter recordings with the encoder model using only 30-second ECG inputs, it was found that DeepHHF improved risk stratification. The encoder model yielded higher NNSs of 32 and 23 for moderate- and high-risk subgroups, respectively, compared to NNSs of 30 and 21 for DeepHHF. These findings suggest that DeepHHF has the potential to optimize resource utilization and enhance clinical outcomes by focusing preventive care on patients most likely to benefit from it.

This research had several limitations. First, despite the large dataset used for the experiments and the fact that the ECG data was collected in 20 different primary care facilities, the model should be evaluated in other centers around the world to cover a wider range of ethnicity, comorbidities, and medical center practices. In this work, an additional dataset from Rambam Health Care Campus (Haifa, Israel) was obtained to support the external validation of our model. However, this dataset is of moderate size and may have limited variability, potentially reducing its ability to represent populations that differ substantially from the internal cohort. Furthermore, the large cohort used in this research was not defined based on systematic clinical or demographic information, and therefore other Holter ECG samples may be different with varying clinical practice and policy of the healthcare system. This further emphasizes the importance of using external test sets in future work. Moreover, this study includes an inherent selection bias due to the use of Holter monitoring, which is typically performed for specific clinical indications. While this reflects real-world primary care practice, it may limit the generalizability of the findings to specific cardiovascular subgroups.

An additional limitation of this study was that the predicted HF outcome was restricted to specific clinically documented stages of the disease, as recorded by physicians, rather than covering the full spectrum of possible HF presentations, including asymptomatic or atypical cases. This narrow focus may limit the ability of the model to detect earlier or less clearly defined stages of HF that are often missing from clinical records. However, these milder cases are generally associated with a lower clinical burden. One additional important limitation of our study is the absence of a direct comparison between the predictive value of Holter ECG and 12-lead ECG for HF risk prediction. Indeed, while this research provided valuable empirical evidence supporting the value of long-term (24-hour) versus short-term (30-second) ECG recordings, these comparisons were based on single-lead recordings. Moreover, the use of trimmed or zero-padded recordings to match a 24-hour input length was intended to simplify the model design. Given the tight distribution of recording durations (mean = 24.67h, median = 23.79h, IQR = 1.44h), it is reasonable to assume that any potential bias was mitigated by the large size of the dataset.

Additional improvements may be achieved through recently developed open ECG foundation models [39–43] which can be exploited and fine-tuned for potentially improved performance of the downstream HF risk prediction task.

Methods

Technion-Leumit Holter ECG dataset elaboration

The TLHE dataset was developed in partnership with the Israeli HMO Leumit. Leumit Health Services is one of the four HMOs active in Israel and provides medical services to more than 725,000 active members. The HMO has a comprehensive online computerized EMR database of all of its current and past members. Medical data from 2003 and onward are and have been collected from over 1.2 million individuals, allowing for a follow-up of up to 20 years. Leumit's EMR database includes data from primary and specialist community care providers, hospital admissions, laboratory test results, and pharmacies. Continuously updated mortality information was available from the national population registry. In addition to the EMR database, Leumit has access to raw Holter ECG data from corresponding patient examinations. This research

included all Leumit patients with available Holter ECG recordings between 2010 and June 2023. The demographic and clinical information for the cohort is summarized in Table 1.

The EMR data used was last updated on April 2024. Exclusion criteria (Figure 2) included corrupted files that could not be decoded from their binary format, recording duration below 20 hours, failure in mapping between the Holter recording and the patient EMR data, recordings from individuals under 18 years old. In addition, Holters timestamped with an inconsistent date, considered as outliers or wrongly dated, were excluded, i.e., Holters dated before 2010, which is when digitally storage of Holter data only began, or after 2023, that is after the inclusion period (see Extended Data Fig. 6). Since our research interest is in risk prediction, all Holter recordings that had a diagnosis for HF documented prior to the Holter examination were discarded.

The following variables were extracted from the EMR: patient demographics, body mass index (BMI), smoking status, medical diagnoses from both the clinic and hospital, hospital admissions, emergency department visits, clinic visits, lab results, measures (e.g., blood pressure), procedures, medication prescriptions and consumption, and death date. Data on hospital diagnoses were available starting from 2018. All diagnosis data were documented with ICD-9 codes. Prescribed medications were coded according to the Anatomical Therapeutic Chemical (ATC) Classification system. All events were dated with an absolute date.

All Holter examinations, including patient preparation, placement of the device, and returning the device, were performed in one of 20 Leumit primary care facilities by Leumit nurses. Leumit patients may be referred for Holter examination by primary care physicians or cardiologists, with primary indications including syncope evaluation, assessment of palpitations or irregular heart rhythm, and the evaluation and follow-up of patients with known arrhythmias. The ECGs were remotely interpreted by certified cardiologists in a centralized private clinic. The Holter ECGs were recorded using the Lifecard CF device (Spacelabs Healthcare) and included 3 leads. On average, Holter recordings lasted for 24-hour. ECGs were originally sampled at 1024Hz and downsampled to 128Hz by the device with a dynamic range of $\pm 5\text{mV}$ and a resolution of $2.5\mu\text{V}$. The electrode positions for the single lead used in this research followed manufacturer's instructions: right sternal border at the level of the 2nd rib (-) and left anterior axillary lines and on the 6th ribs (+).

Information connecting between the recordings and the EMR data, in addition to complementary metadata, such as the recording date and the daytime hour of the recording start, was extracted from the binary files before de-identification. Respectively, the identifying data for the recordings was encoded in the same manner as the EMR data. Patient data were de-identified according to HMO standards and in accordance with the Israel Ministry of Health guidelines. In particular, the patient's ID and address as well as the physician's ID were encrypted and the date of birth was removed, leaving only the year of birth.

Class definition

The endpoint was defined as the first documented diagnosis for HF in the EMR, as reported by the physician during a medical visit (clinic, emergency room or hospital). Accordingly, the endpoint date was defined as the first date out of any of the HF diagnoses documented for the patient. The ICD-9 codes that were used to identify HF diagnosis in the EMR are listed in Extended Data Table A1. These were selected after consulting with the Leumit director of family medicine (co-author IG), to ensure inclusion of all possible codes that appear as "Heart failure" in the doctors' electronic system interface, or codes that could have been given during hospitalization. To verify the validity of the HF diagnosis endpoints, several methods also used in previous research [23] were used, as described in Extended Data section A.1. Each Holter recording was labeled as HF if an HF diagnosis was documented within 5-year of the examination. In contrast, Holter recordings that did not have a HF diagnosis documented within 5 years from the recording were labeled as non-HF (Figure 2).

Dataset split and preprocessing

After applying the exclusion criteria and defining the labels, the recordings were divided into train, validation and test sets. The test set was comprised of all recordings from the first four months (January-April) of 2018. This period was selected because it marked the earliest availability of hospital diagnosis data, ensuring the reference labels for HF were as comprehensive and reliable as possible. Additionally, it allowed for at least a 5-year follow-up, as clinical data extended through April 2024. To avoid information leakage, a stratification step was applied, in which all patient recordings of those who had a recording performed within this time frame (January-April 2018) were also included in the test set. Subsequently, 5% of the remaining recordings were randomly selected to form the validation set and the same patient stratification step was applied. The remaining recordings were allocated to the train set. This process resulted in 48,013, 5,101, and 4,461 recordings from 35,884, 2,626, and 2,105 patients for the train, validation and test sets, respectively. The first lead out of three from each recording was used for all the experiments. To standardize the dataset, the length of the Holter recordings was adjusted to 24 hours, either by trimming excess data or by zero-padding shorter recordings.

Deep learning model

The DL model was trained in two steps (Figure 6). In the first step, in each epoch, 30-second windows (3,840 samples) were randomly sampled once every 3-minute segment in the Holter recordings. This resulted in 480 windows per recording. These windows were used to train an encoder for the binary classification task of interest. Correspondingly, fully connected

Table 1: Study cohort characteristics. Holter examinations are divided into train and test sets and by whether they belong to the positive class (HF) or negative class (non-HF).

		Train set		Test set	
		non-HF (n=49,998)	HF (n=3,116)	non-HF (n=4,135)	HF (n=326)
Age at recording	18-39	8,855 (17.71%)	24 (0.77%)	408 (9.87%)	1 (0.31%)
	40-49	5,734 (11.47%)	81 (2.6%)	318 (7.69%)	6 (1.84%)
	50-59	8,450 (16.9%)	227 (7.29%)	584 (14.12%)	17 (5.21%)
	60-69	12,207 (24.42%)	675 (21.68%)	1,271 (30.74%)	65 (19.94%)
	70-79	10,362 (20.73%)	1,179 (37.87%)	1,103 (26.67%)	119 (36.5%)
	80+	4,387 (8.77%)	927 (29.78%)	451 (10.91%)	118 (36.2%)
Sex	F	30,583 (61.17%)	1,579 (50.67%)	2,609 (63.1%)	207 (63.5%)
	M	19,409 (38.82%)	1,537 (49.33%)	1,526 (36.9%)	119 (36.5%)
Year at recording	2010-2018	25,452 (50.91%)	1,801 (57.8%)	1,090 (26.36%)	61 (18.71%)
	2018-2024	24,546 (49.09%)	1,315 (42.2%)	3,045 (73.64%)	265 (81.29%)
BMI	0-18.5	840 (1.79%)	28 (0.96%)	69 (1.69%)	0 (0.0%)
	18.5-25	13,885 (29.53%)	513 (17.6%)	972 (23.78%)	44 (13.54%)
	25-30	17,924 (38.12%)	1,125 (38.59%)	1,571 (38.44%)	116 (35.69%)
	30-35	9,835 (20.92%)	762 (26.14%)	1,035 (25.32%)	104 (32.0%)
	35-40	3,269 (6.95%)	332 (11.39%)	311 (7.61%)	34 (10.46%)
	40+	1,267 (2.69%)	155 (5.32%)	129 (3.16%)	27 (8.31%)
Smoking	Not smoking	40,878 (81.76%)	2,705 (86.81%)	3,575 (86.46%)	308 (94.48%)
	Previously/currently	8,308 (16.62%)	371 (11.91%)	543 (13.13%)	18 (5.52%)
	Unknown	812 (1.62%)	40 (1.28%)	17 (0.41%)	0 (0.0%)
	Diabetes	11,634 (23.27%)	1,308 (41.98%)	1,091 (26.38%)	126 (38.65%)
Comorbidities at/before recording	Ischemic heart disease	Any	13,352 (26.71%)	1,748 (56.1%)	1,315 (31.8%)
		MI or acute coronary event	2,846 (5.69%)	541 (17.36%)	252 (6.09%)
		Other	12,718 (25.44%)	1,653 (53.05%)	1,264 (30.57%)
	Cerebrovascular disease	Any	9,759 (19.52%)	1,017 (32.64%)	1,022 (24.72%)
		Stroke	7,447 (14.89%)	759 (24.36%)	725 (17.53%)
		Chronic renal failure	2,010 (4.02%)	425 (13.64%)	242 (5.85%)
	Cardiac dysrhythmia	Acute renal failure	232 (0.46%)	62 (1.99%)	35 (0.85%)
		Cardiac conduction disorder	2,450 (4.9%)	340 (10.91%)	283 (6.84%)
		Any	16,012 (32.03%)	1,790 (57.45%)	2,050 (49.58%)
	Hypertension	Atrial fibrillation/flutter	7,322 (14.64%)	1,225 (39.31%)	1,153 (27.88%)
		Ventricular tachycardia	823 (1.65%)	92 (2.95%)	128 (3.1%)
		Valvular heart disease	25,985 (51.97%)	2,607 (83.66%)	2,604 (62.97%)
	Chronic obstructive pulmonary disease	Chronic hypertension	4,902 (9.8%)	650 (20.86%)	616 (14.9%)
		Cancer	18,117 (36.24%)	1,473 (47.27%)	1,742 (42.13%)
			6,864 (13.73%)	663 (21.28%)	693 (16.76%)
					81 (24.85%)

layers (FCs, Figure 6) were used to classify the extracted features of each 30-second window independently. In the second step, the 30-second windows were sampled for every 2-minute segment, resulting in 720 windows per recording. In this step, the trained encoder was frozen and used as a feature generator for each 30-second windows, to train the sequential head. The extracted features were connected from the different windows to form a sequential representation of the entire 24-hour ECG recording, and to be processed by the sequential head. Then the processed sequence went through FCs (different weights than the encoder FCs) for the final whole Holter classification. Thus, in summary, the DeepHHF model generates a score for the entire Holter recording based on the extracted features.

The architecture of both parts of the model is summarized in Extended Data Fig. 9. The encoder basic building block was adapted from the EnCodec architecture [44]. The motivation behind this choice was to create a low-dimensional compact representation in the latent space. These were passed to the second training step, enabling a large number of encoded 30-second windows to be included while considering the entire 24-hour recording. In summary, this building block consisted of a residual block, following a strided convolutional layer, thereby substantially reducing the dimensions after each block. Overall, the encoder consisted of four building blocks, followed by two FC layers. The sequential head was built from a transformer encoder followed by two FC layers. For both steps, the loss function used was a class-weighted binary cross-entropy, with class weights calculated based on the proportion of positive to negative labels in the train set. The loss function was integrated with a sigmoid function to obtain probabilities at the FCs output. A learning rate of 10^{-3} was used in the first step, as attempts with different rates did not yield better convergence, whereas in the second step a learning rate of 5×10^{-5} was used after hyperparameters search. An unlimited number of epochs was used, with early stopping applied after eight consecutive epochs with no improvement. Improvement was measured based on the AUROC over the validation set. The DL pipeline was implemented via PyTorch version 2.2.2 with Python version 3.8.19. All computations were executed on Microsoft Azure using the NC48ads A100 v4 instance (48 vCPUs, 440 GiB memory). A batch size of 32 was used in both training steps, which was tuned to maximize the memory allocation in the GPU during training.

Hyperparameters were optimized using Bayesian search via Optuna [45] version 3.6.1. The optimization attempted to maximize the validation set AUROC score. For the encoder, the filter size of first convolution layer, size of strides and corresponding convolution filter size of the final layer inside the building block, the number of filters (same for all convolutional layers), and the dropout rate p were tuned. For the sequential head, the segment size to sample the 30-second windows from (was tuned to 2 minutes, see Figure 6), and the learning rate, transformer d_{model} , number of heads

in the transformer attention layers, number of transformer encoder layers, and the feedforward dimension (transformer linear layer size) were tuned.

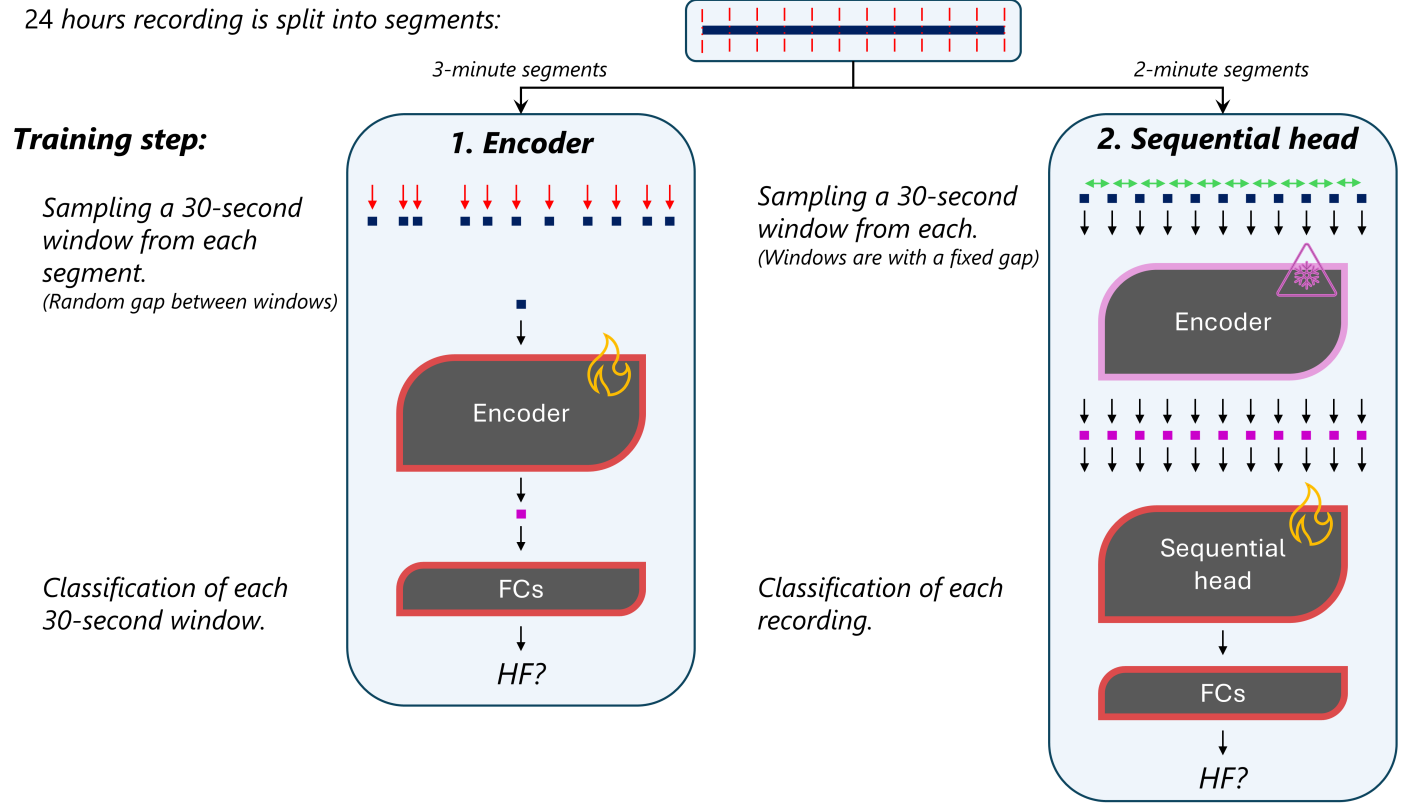


Fig. 6: The two training steps and the window sampling technique in each. **Step 1 - training the encoder:** The 24-hour recording is split into 3-minute segments, and a 30-second window is sampled from each segment. The gap between the windows is random. The fully-connected layers (FCs) output a HF score for each individual window. **Step 2 - training the sequential head:** The 24-hour recording is split into 2-minute segments and the gap between the 30-second windows is fixed, forming a sequence. The encoder's weights are frozen and it is used for feature extraction. The FCs (different set) output a HF score for the entire recording.

Rambam Holter databank cohort for external validation

To evaluate the generalization performance of the model on an independent external test set, data were obtained from the Holter databank (IRB number: 0057-23-RMB-D) of Rambam Health Care Campus, a secondary care medical center in Haifa, Israel. Holter recordings collected between 2017 and 2018 were extracted from individuals over 30 years of age who did not have a pacemaker and were not receiving cardiac pharmacological treatment at the time of examination. Clinical follow-up data were available through November 2021. In total, 150 Holter examinations were included, comprising 29 from patients who were subsequently diagnosed with HF and 121 from patients without documented future HF (Non-HF).

PCP-HF score computation

The PCP-HF clinical score was calculated using the equation parameters reported by Khan et al. [17] (in their Table 2) for the estimation of the 10-year risk of HF. The score was also validated for 5-year risk prediction based on other Israeli HMO EMR extracted data [23]. Since individuals with black skin make up less than 2% of the total population in Israel [46], only the white male and female coefficients were used, similarly to Khan et al [23]. Patient age at the time of Holter examination and smoking history were obtained from the Leumit EMR patient's demographic file. BMI and systolic blood pressure were extracted from the EMR measures file. Glucose, cholesterol, and high-density lipoprotein cholesterol (HDL-C) levels were extracted from the patient's laboratory results file. The measurement and laboratory results closest to the Holter index date, which were documented within a window of two years before to two months after this date, were used. Treatments for diabetes and hypertension were defined by at least one dispensed prescription of a relevant medication (based on ATC codes as per Khan et al. [23]) within the same time frame as the measurements and laboratory results. To measure the duration of the QRS complex, the QRS durations from the first five minutes of the ECG of the twelfth recording hour, that is, about the middle of the recording, were averaged. This process involved filtering the signal, detecting R-peaks and R-on and R-off fiducials using the NeuroKit2 [47] version 0.2.9, and calculating

the difference between R-off and R-on for each detected R-peak. For systolic blood pressure and glucose, the untreated coefficients were used. If any variable was missing for a given recording, then it was excluded from the ROC curve computation. Consequently, 1,917 out of 4,461 cases in the test were considered.

Model explainability analysis

The model explainability analysis was performed using gradient attention rollout [18, 19]. The technique involved modification of the original vision transformer code and its adaptation to 1D time-series signals. Accordingly, the multi-head attention from each transformer encoder layer (Extended Data Figure 9) was extracted and weighted by its gradient. These were accumulated to a single attention across all the encoder layers. The different heads were averaged, and a discard ratio of 0.9 was applied, as suggested in the original technique, simplifying visualization and analysis.

To study the circadian component of DeepHFF, the attention density across all HF and non-HF recordings in the test set was analyzed. Unsupervised learning was employed to evaluate the characteristics of beats identified by DeepHFF. Time intervals with high DeepHFF attention were identified for all test set recordings classified as HF. For each of these intervals, a 10-second segment was retained, and R-peaks were detected using the jqr peak detector [48, 49]. Beats were then segmented with 50 samples on either side of the R-peak, resulting in beat lengths of 0.78ms. K-means clustering was then applied to the segmented beats and silhouette analysis was used to determine the optimal number of clusters. Only clusters with a minimum of 30 beats were retained. Finally, t-SNE was employed for visualization. The K-means, silhouette and t-SNE algorithms were applied using scikit-learn [50] version 1.3.0.

Kaplan-Meier curves

Three HF risk groups were defined: low, moderate, and high risk. Moderate risk was defined by the probability threshold that yields a specificity of 70% and high risk by the probability threshold that yields a specificity of 90%. Due to the low proportion of HF patients in the cohort, high specificity is needed to limit the number of FP. Figure 3c shows the probability decision threshold associated with this definition.

The clinical value of DeepHFF was assessed by evaluating survival of the high risk group vs. low/moderate-risk group (Figure 3c). The Kaplan-Meier curves were plotted with respect to the Holter examination dates for the test set. Two survival analyses were performed: one with respect to death incidents, and the second with respect to either documented hospitalization admissions in cardiac and internal departments or death incidents. For an Holter examination, the time interval between the examination date and a follow-up hospitalization and death event were calculated. The date of the latest documented event for all individuals in the test set was used for censorship. Survival curves were produced both for the TP, FP, TN and FN groups as well as for the different risk groups. For the latest, the odds ratios between the high and moderate/low groups were computed. The encoder model survival curves were produced as well for the risk groups the same manner. The Kaplan-Meier curves were generated using the lifelines [51] version 0.27.8.

Performance measures and statistical analysis

The predictive performance of the obtained classifiers was measured by the AUROC determined with the test set. The AUROC CI was estimated by bootstrapping for 1,000 iterations over the test set. Specifically, in each iteration, an AUROC was calculated for a random subset comprised of 250 non-HF examples and 250 HF examples, resulting in a total of 500 examples from the test set. The statistical significance between two classifiers was obtained using a Student's t-test between the bootstrapped test set distributions. To compare and evaluate the statistical significance between two Kaplan-Meier curves, the logrank test was applied using the lifelines [51] version 0.27.8. For all statistical tests, significance was set at p -value < 0.05 . For all CIs, the confidence level was determined at 95%.

Declarations

Acknowledgments: We thank Nuriel Burak from Leumit Health Services for his invaluable support in exporting and maintaining the data from the HMO systems, as well as for his assistance in supporting the computing system throughout the project.

Funding: EZ acknowledges The Miriam and Aaron Gutwirth Memorial Fellowship. EZ and JB acknowledge the Technion EVPR Fund: Hittman Family Fund. The research was supported by a cloud computing grant from the Israel Council of Higher Education, administered by the Israel Data Science Initiative. We acknowledge the assistance of ChatGPT, an AI-based language model developed by OpenAI, for its help in editing the English language of this manuscript.

Data availability: All requests for raw data can be addressed to Leumit Start (co-author IL). Any data and materials that can be shared will be released via the standard Data Transfer Agreement of the Leumit Health Maintenance Organization. Source Data are provided with this paper.

Author contribution: JB and EZ conceived and designed the research. EZ developed the dataset and algorithms and performed the analysis under the supervision of JB. RA guided the epidemiological methodological design and heart failure label verification. OA, MG, RA and IG provided medical guidance on interpreting the data and the clinical outlook

of the research. IL supported the development of the dataset, data curation, data management and cloud computing platform. JB and EZ drafted the first version of the manuscript. All authors edited and revised the manuscript and approved the final version.

Ethics approval and consent to participate: The study protocol was approved by the statutory Leumit Health Services Institutional Review Board (approval number 0025-22 LEU). Informed consent was waived because this large-scale retrospective study was performed on deidentified electronic health records.

Code availability: The experiments can be reproduced by utilizing the details provided in the Methods section. For DeepHHF, this includes the model architecture (Extended Data Figure 9). Our trained model is also made publicly available at (URL upon publication) and is provided for academic research purposes and under a GNU GPL license. Main Python package versions: Python - 3.8.19; PyTorch - 2.2.2; scikit-learn - 1.3.0; lifelines - 0.27.8; Optuna - 3.6.1; NeuroKit2 - 0.2.9.

Conflict of interest: the authors declare no conflict of interest.

References

- [1] Groenewegen, A., Rutten, F.H., Mosterd, A., Hoes, A.W.: Epidemiology of heart failure. *European Journal of Heart Failure* **22**(8), 1342–1356 (2020) <https://doi.org/10.1002/ejhf.1858>
- [2] Rossignol, P., Hernandez, A.F., Solomon, S.D., Zannad, F.: Heart failure drug treatment. *The Lancet* **393**(10175), 1034–1044 (2019) [https://doi.org/10.1016/S0140-6736\(18\)31808-7](https://doi.org/10.1016/S0140-6736(18)31808-7)
- [3] Heidenreich, P.A., Bozkurt, B., Aguilar, D., Allen, L.A., Byun, J.J., Colvin, M.M., Deswal, A., Drazner, M.H., Dunlay, S.M., Evers, L.R., Fang, J.C., Fedson, S.E., Fonarow, G.C., Hayek, S.S., Hernandez, A.F., Khazanie, P., Kittleson, M.M., Lee, C.S., Link, M.S., Milano, C.A., Nnacheta, L.C., Sandhu, A.T., Stevenson, L.W., Vardeny, O., Vest, A.R., Yancy, C.W.: 2022 AHA/ACC/HFSA guideline for the management of heart failure: A report of the American College of Cardiology/American Heart Association Joint Committee on Clinical Practice Guidelines. *Circulation* **145**(18), 895–1032 (2022) <https://doi.org/10.1161/CIR.0000000000001063>
- [4] Bennett, J.A., Riegel, B., Bittner, V., Nichols, J.: Validity and reliability of the NYHA classes for measuring research outcomes in patients with cardiac disease. *Heart & Lung* **31**(4), 262–270 (2002) <https://doi.org/10.1067/mhl.2002.124554>
- [5] Bozkurt, B., Coats, A.J., Tsutsui, H., Abdelhamid, M., Adamopoulos, S., Albert, N., Anker, S.D., Atherton, J., Böhm, M., Butler, J., Drazner, M.H., Felker, G.M., Filippatos, G., Fonarow, G.C., Fiuzat, M., Gomez-Mesa, J.E., Heidenreich, P., Imamura, T., Januzzi, J., Jankowska, E.A., Khazanie, P., Kinugawa, K., Lam, C.S.P., Matsue, Y., Metra, M., Ohtani, T., Francesco Piepoli, M., Ponikowski, P., Rosano, G.M.C., Sakata, Y., Seferović, P., Starling, R.C., Teerlink, J.R., Vardeny, O., Yamamoto, K., Yancy, C., Zhang, J., Zieroth, S.: Universal definition and classification of heart failure: A report of the Heart Failure Society of America, Heart Failure Association of the European Society of Cardiology, Japanese Heart Failure Society and Writing Committee of the Universal Definition o. *Journal of Cardiac Failure* **27**(4), 387–413 (2021) <https://doi.org/10.1016/J.CARDFAIL.2021.01.022>
- [6] Benjamin, E.J., Blaha, M.J., Chiuve, S.E., Cushman, M., Das, S.R., Deo, R., De Ferranti, S.D., Floyd, J., Fornage, M., Gillespie, C., Isasi, C.R., Jim'nez, M.C., Jordan, L.C., Judd, S.E., Lackland, D., Lichtman, J.H., Lisabeth, L., Liu, S., Longenecker, C.T., MacKey, R.H., Matsushita, K., Mozaffarian, D., Mussolini, M.E., Nasir, K., Neumar, R.W., Palaniappan, L., Pandey, D.K., Thiagarajan, R.R., Reeves, M.J., Ritchey, M., Rodriguez, C.J., Roth, G.A., Rosamond, W.D., Sasson, C., Towfighi, A., Tsao, C.W., Turner, M.B., Virani, S.S., Voeks, J.H., Willey, J.Z., Wilkins, J.T., Wu, J.H.Y., Alger, H.M., Wong, S.S., Muntner, P.: Heart disease and stroke statistics'2017 update: A report from the American Heart Association. *Circulation* **135**(10), 146–603 (2017) <https://doi.org/10.1161/CIR.0000000000000485/ASSET/065F105B-352E-48D3-AC2B-2F0A69AE4BE0/ASSETS/CIR.0000000000000485.FP.PNG>
- [7] Wang, H., Gao, C., Guignard-Duff, M., Cole, C., Hall, C., Larman, M., Baruah, R., Gao, H., Mamza, J.B., Lang, C.C., Mordi, I.: Importance of early diagnosis and treatment of heart failure across the spectrum of ejection fraction. *European Heart Journal* **44**(Supplement_2), 655–892 (2023) <https://doi.org/10.1093/eurheartj/ehad655.892>
- [8] Ribeiro, A.H., Ribeiro, M.H., Paixão, G.M.M., Oliveira, D.M., Gomes, P.R., Canazart, J.A., Ferreira, M.P.S., Andersson, C.R., Macfarlane, P.W., Meira, W., Schön, T.B., Ribeiro, A.L.P.: Automatic diagnosis of the 12-lead ECG using a deep neural network. *Nature Communications* **11**(1), 1760–1760 (2020) <https://doi.org/10.1038/s41467-020-15432-4>
- [9] Biton, S., Gendelman, S., Ribeiro, A.H., Miana, G., Moreira, C., Ribeiro, A.L.P., Behar, J.A.: Atrial fibrillation risk prediction from the 12-lead electrocardiogram using digital biomarkers and deep representation learning. *European Heart Journal - Digital Health* **2**(4), 576–585 (2021) <https://doi.org/10.1093/EHJDH/ZTAB071>

[10] Al-Zaiti, S.S., Martin-Gill, C., Zègre-Hemsey, J.K., Bouzid, Z., Faramand, Z., Alrawashdeh, M.O., Gregg, R.E., Helman, S., Riek, N.T., Kraevsky-Phillips, K., Clermont, G., Akcakaya, M., Sereika, S.M., Van Dam, P., Smith, S.W., Birnbaum, Y., Saba, S., Sejdic, E., Callaway, C.W.: Machine learning for ECG diagnosis and risk stratification of occlusion myocardial infarction. *Nature Medicine* **29**, 1804–1813 (2023) <https://doi.org/10.1038/s41591-023-02396-3>

[11] Holmstrom, L., Christensen, M., Yuan, N., Weston Hughes, J., Theurer, J., Jujjavarapu, M., Fatehi, P., Kwan, A., Sandhu, R.K., Ebinger, J., Cheng, S., Zou, J., Chugh, S.S., Ouyang, D.: Deep learning-based electrocardiographic screening for chronic kidney disease. *Communications Medicine* **3**, 73–73 (2023) <https://doi.org/10.1038/s43856-023-00278-w>

[12] Attia, Z.I., Kapa, S., Lopez-Jimenez, F., McKie, P.M., Ladewig, D.J., Satam, G., Pellikka, P.A., Enriquez-Sarano, M., Noseworthy, P.A., Munger, T.M., Asirvatham, S.J., Scott, C.G., Carter, R.E., Friedman, P.A.: Screening for cardiac contractile dysfunction using an artificial intelligence-enabled electrocardiogram. *Nature Medicine* **25**(1), 70–74 (2019) <https://doi.org/10.1038/s41591-018-0240-2>

[13] Attia, Z.I., Kapa, S., Yao, X., Lopez-Jimenez, F., Mohan, T.L., Pellikka, P.A., Carter, R.E., Shah, N.D., Friedman, P.A., Noseworthy, P.A.: Prospective validation of a deep learning electrocardiogram algorithm for the detection of left ventricular systolic dysfunction. *Journal of Cardiovascular Electrophysiology* **30**(5), 668–674 (2019) <https://doi.org/10.1111/JCE.13889>

[14] Dunlay, S.M., Roger, V.L., Redfield, M.M.: Epidemiology of heart failure with preserved ejection fraction. *Nature Reviews Cardiology* **14**(10), 591–602 (2017) <https://doi.org/10.1038/nrcardio.2017.65>

[15] Khan, M.S., Shahid, I., Bennis, A., Rakisheva, A., Metra, M., Butler, J.: Global epidemiology of heart failure. *Nature Reviews Cardiology* **21**(10), 717–734 (2024) <https://doi.org/10.1038/s41569-024-01046-6>

[16] Prinzen, F.W., Auricchio, A., Mullens, W., Linde, C., Huizar, J.F.: Electrical management of heart failure: from pathophysiology to treatment. *European Heart Journal* **43**(20), 1917–1927 (2022) <https://doi.org/10.1093/eurheartj/ehac088>

[17] Khan, S.S., Ning, H., Shah, S.J., Yancy, C.W., Carnethon, M., Berry, J.D., Mentz, R.J., O'Brien, E., Correa, A., Suthahar, N., Boer, R.A., Wilkins, J.T., Lloyd-Jones, D.M.: 10-Year risk equations for incident heart failure in the general population. *Journal of the American College of Cardiology* **73**(19), 2388–2397 (2019) <https://doi.org/10.1016/j.jacc.2019.02.057>

[18] Abnar, S., Zuidema, W.: Quantifying attention flow in transformers. In: Proceedings of the 58th Annual Meeting of the Association for Computational Linguistics, pp. 4190–4197. Association for Computational Linguistics, Online (2020). <https://doi.org/10.18653/v1/2020.acl-main.385>

[19] Gildenblat, J.: Exploring Explainability for Vision Transformers (2020). <https://jacobgil.github.io/deeplearning/vision-transformer-explainability>

[20] Khurshid, S., Friedman, S., Reeder, C., Di Achille, P., Diamant, N., Singh, P., Harrington, L.X., Wang, X., Al-Alusi, M.A., Sarma, G., Foulkes, A.S., Ellinor, P.T., Anderson, C.D., Ho, J.E., Philippakis, A.A., Batra, P., Lubitz, S.A.: ECG-based deep learning and clinical risk factors to predict atrial fibrillation. *Circulation* **145**(2), 122–133 (2022) <https://doi.org/10.1161/CIRCULATIONAHA.121.057480>

[21] Prifti, E., Fall, A., Davogustto, G., Pulini, A., Denjoy, I., Funck-Brentano, C., Khan, Y., Durand-Salmon, A., Badilini, F., Wells, Q.S., Leenhardt, A., Zucker, J.D., Roden, D.M., Extramiana, F., Salem, J.E.: Deep learning analysis of electrocardiogram for risk prediction of drug-induced arrhythmias and diagnosis of long QT syndrome. *European Heart Journal* **42**(38), 3948–3961 (2021) <https://doi.org/10.1093/EURHEARTJ/EHAB588>

[22] Hughes, J.W., Tooley, J., Torres Soto, J., Ostropolets, A., Poterucha, T., Christensen, M.K., Yuan, N., Ehlert, B., Kaur, D., Kang, G., Rogers, A., Narayan, S., Elias, P., Ouyang, D., Ashley, E., Zou, J., Perez, M.V.: A deep learning-based electrocardiogram risk score for long term cardiovascular death and disease. *npj Digital Medicine* **6**, 169–169 (2023) <https://doi.org/10.1038/s41746-023-00916-6>

[23] Khan, S.S., Barda, N., Greenland, P., Dagan, N., Lloyd-Jones, D.M., Balicer, R., Rasmussen-Torvik, L.J.: Validation of heart failure-specific risk equations in 1.3 million Israeli adults and usefulness of combining ambulatory and hospitalization data from a large integrated health care organization. *The American Journal of Cardiology* **168**, 105–109 (2022) <https://doi.org/10.1016/j.amjcard.2021.12.017>

[24] Sinha, A., Gupta, D.K., Yancy, C.W., Shah, S.J., Rasmussen-Torvik, L.J., McNally, E.M., Greenland, P., Lloyd-Jones, D.M., Khan, S.S.: Risk-based approach for the prediction and prevention of heart failure. *Circulation: Heart*

Failure **14**(2), 007761 (2021) <https://doi.org/10.1161/CIRCHEARTFAILURE.120.007761>

- [25] Dhingra, L.S., Aminorroaya, A., Sangha, V., Pedroso, A.F., Asselbergs, F.W., Brant, L.C.C., Barreto, S.M., Ribeiro, A.L.P., Krumholz, H.M., Oikonomou, E.K., Khera, R.: Heart failure risk stratification using artificial intelligence applied to electrocardiogram images: a multinational study. *European Heart Journal* **46**(11), 1044–1053 (2025) <https://doi.org/10.1093/eurheartj/ehae914> . Accessed 2025-07-12
- [26] Butler, L., Karabayir, I., Kitzman, D.W., Alonso, A., Tison, G.H., Chen, L.Y., Chang, P.P., Clifford, G., Soliman, E.Z., Akbilgic, O.: A generalizable electrocardiogram-based artificial intelligence model for 10-year heart failure risk prediction. *Cardiovascular Digital Health Journal* **4**(6), 183–190 (2023) <https://doi.org/10.1016/j.cvdhj.2023.11.003> . Accessed 2025-07-12
- [27] Akbilgic, O., Butler, L., Karabayir, I., Chang, P.P., Kitzman, D.W., Alonso, A., Chen, L.Y., Soliman, E.Z.: ECG-AI: electrocardiographic artificial intelligence model for prediction of heart failure. *European Heart Journal - Digital Health* **2**(4), 626–634 (2021) <https://doi.org/10.1093/ehjdh/ztab080> . Accessed 2025-07-12
- [28] Phan, H., Andreotti, F., Cooray, N., Chén, O.Y., De Vos, M.: SeqSleepNet: End-to-End Hierarchical Recurrent Neural Network for Sequence-to-Sequence Automatic Sleep Staging. *IEEE Transactions on Neural Systems and Rehabilitation Engineering* **27**(3), 400–410 (2019) <https://doi.org/10.1109/TNSRE.2019.2896659> . Accessed 2025-07-05
- [29] Lin, C.-S., Liu, W.-T., Tsai, D.-J., Lou, Y.-S., Chang, C.-H., Lee, C.-C., Fang, W.-H., Wang, C.-C., Chen, Y.-Y., Lin, W.-S., Cheng, C.-C., Lee, C.-C., Wang, C.-H., Tsai, C.-S., Lin, S.-H., Lin, C.: AI-enabled electrocardiography alert intervention and all-cause mortality: a pragmatic randomized clinical trial. *Nature Medicine* **30**(5), 1461–1470 (2024) <https://doi.org/10.1038/s41591-024-02961-4> . Publisher: Nature Publishing Group. Accessed 2024-11-01
- [30] Jain, S., Wallace, B.C.: Attention is not Explanation. *arXiv. arXiv:1902.10186 [cs]* (2019). <https://doi.org/10.48550/arXiv.1902.10186> . <http://arxiv.org/abs/1902.10186> Accessed 2025-07-04
- [31] Chefer, H., Gur, S., Wolf, L.: Transformer Interpretability Beyond Attention Visualization, pp. 782–791 (2021)
- [32] Jo, S., Jang, G., Park, H.: GMAR: Gradient-Driven Multi-Head Attention Rollout for Vision Transformer Interpretability. *arXiv. arXiv:2504.19414 [cs]* (2025). <https://doi.org/10.48550/arXiv.2504.19414> . <http://arxiv.org/abs/2504.19414> Accessed 2025-07-04
- [33] Portaluppi, F., Hermida, R.C.: Circadian rhythms in cardiac arrhythmias and opportunities for their chronotherapy. *Advanced Drug Delivery Reviews* **59**(9-10), 940–951 (2007) <https://doi.org/10.1016/J.ADDR.2006.10.011>
- [34] Dukes, J.W., Dewland, T.A., Vittinghoff, E., Mandyam, M.C., Heckbert, S.R., Siscovick, D.S., Stein, P.K., Psaty, B.M., Sotoodehnia, N., Gottdiener, J.S., Marcus, G.M.: Ventricular ectopy as a predictor of heart failure and death. *Journal of the American College of Cardiology* **66**(2), 101–109 (2015) <https://doi.org/10.1016/J.JACC.2015.04.062>
- [35] Maisel, W.H., Stevenson, L.W.: Atrial fibrillation in heart failure: epidemiology, pathophysiology, and rationale for therapy. *The American Journal of Cardiology* **91**(6), 2–8 (2003) [https://doi.org/10.1016/S0002-9149\(02\)03373-8](https://doi.org/10.1016/S0002-9149(02)03373-8)
- [36] Bergau, L., Bengel, P., Sciacca, V., Fink, T., Sohns, C., Sommer, P.: Atrial fibrillation and heart failure. *Journal of Clinical Medicine* **11**(9), 2510–2510 (2022) <https://doi.org/10.3390/JCM11092510>
- [37] Ledwidge, M., Gallagher, J., Conlon, C., Tallon, E., O'Connell, E., Dawkins, I., Watson, C., O'Hanlon, R., Birmingham, M., Patle, A., Badabagni, M.R., Murtagh, G., Voon, V., Tilson, L., Barry, M., McDonald, L., Maurer, B., McDonald, K.: Natriuretic Peptide-Based Screening and Collaborative Care for Heart Failure: The STOP-HF Randomized Trial. *JAMA* **310**(1), 66–74 (2013) <https://doi.org/10.1001/jama.2013.7588> . Accessed 2024-12-12
- [38] Hernandez, A.F.: Preventing Heart Failure. *JAMA* **310**(1), 44–45 (2013) <https://doi.org/10.1001/jama.2013.7589> . Accessed 2024-12-12
- [39] McKeen, K., Oliva, L., Masood, S., Toma, A., Rubin, B., Wang, B.: ECG-FM: An Open Electrocardiogram Foundation Model. *arXiv* (2024). <https://doi.org/10.48550/ARXIV.2408.05178> . <http://arxiv.org/abs/2408.05178>
- [40] Davies, H.J., Monsen, J., Mandic, D.P.: Interpretable Pre-Trained Transformers for Heart Time-Series Data. *arXiv* (2024). <https://doi.org/10.48550/ARXIV.2407.20775> . <http://arxiv.org/abs/2407.20775>
- [41] Li, J., Aguirre, A., Moura, J., Liu, C., Zhong, L., Sun, C., Clifford, G., Westover, B., Hong, S.: An electrocardiogram foundation model built on over 10 million recordings with external evaluation across multiple domains. *arXiv* (2024).

<https://doi.org/10.48550/arXiv.2410.04133> . <http://arxiv.org/abs/2410.04133>

[42] Guo, Z., Ding, C., Do, D.H., Shah, A., Lee, R.J., Hu, X., Rudin, C.: SiamAF: Learning Shared Information from ECG and PPG Signals for Robust Atrial Fibrillation Detection. arXiv (2024). <https://doi.org/10.48550/ARXIV.2310.09203> . <https://arxiv.org/abs/2310.09203>

[43] Abbaspourazad, S., Elachqar, O., Miller, A.C., Emrani, S., Nallasamy, U., Shapiro, I.: Large-scale Training of Foundation Models for Wearable Biosignals. In: The Twelfth International Conference on Learning Representations - ICLR 2024 (2024). <https://openreview.net/forum?id=pC3WJHf51j>

[44] Défossez, A., Copet, J., Synnaeve, G., Adi, Y.: High Fidelity Neural Audio Compression. Transactions on Machine Learning Research (2023)

[45] Akiba, T., Sano, S., Yanase, T., Ohta, T., Koyama, M.: Optuna: A Next-generation Hyperparameter Optimization Framework. In: Proceedings of the 25th ACM SIGKDD International Conference on Knowledge Discovery & Data Mining. KDD '19, pp. 2623–2631. Association for Computing Machinery, New York, NY, USA (2019). <https://doi.org/10.1145/3292500.3330701>

[46] Israel Central Bureau of Statistics: The Population of Ethiopian Origin in Israel: Selected Data Published on the Occasion of the Sigd Festival 2023. Technical report, Jerusalem (2023). <https://www.cbs.gov.il/en/mediarelease/Pages/2023/The-Ethiopian-Population-in-Israel-2023.aspx>

[47] Makowski, D., Pham, T., Lau, Z.J., Brammer, J.C., Lespinasse, F., Pham, H., Scholzel, C., Chen, S.H.A.: NeuroKit2: A Python toolbox for neurophysiological signal processing. Behavior Research Methods **53**(4), 1689–1696 (2021) <https://doi.org/10.3758/S13428-020-01516-Y/TABLES/3>

[48] Gendelman, S., Biton, S., Derman, R., Zvuloni, E., Levy, J., Lugassy, S., Alexandrovich, A., Behar, J.A.: Physio-Zoo ECG: Digital electrocardiography biomarkers to assess cardiac conduction. In: 2021 Computing in Cardiology (CinC), vol. 2021-September, pp. 1–4. IEEE, Brno, Czech Republic (2021). <https://doi.org/10.23919/CinC53138.2021.9662857>

[49] Behar, J.A., Levy, J., Zvuloni, E., Gendelman, S., Rosenberg, A., Biton, S., Derman, R., A. Sobel, J., Alexandrovich, A., Charlton, P., Marton Aron Goda, D.: PhysioZoo: The Open Physiological Biomarkers Resource. In: Computing in Cardiology. IEEE Computer Society, Atlanta, Georgia, USA (2023). <https://doi.org/10.22489/CinC.2023.190>

[50] Pedregosa, F., Varoquaux, G., Gramfort, A., Michel, V., Thirion, B., Grisel, O., Blondel, M., Prettenhofer, P., Weiss, R., Dubourg, V., Vanderplas, J., Passos, A., Cournapeau, D., Brucher, M., Perrot, M., Duchesnay, E.: Scikit-learn: Machine Learning in Python. Journal of Machine Learning Research **12**(85), 2825–2830 (2011)

[51] Davidson-Pilon, C.: lifelines: survival analysis in Python. Journal of Open Source Software **4**(40), 1317 (2019) <https://doi.org/10.21105/joss.01317>

[52] Goyal, P., Mefford, M.T., Chen, L., Sterling, M.R., Durant, R.W., Safford, M.M., Levitan, E.B.: Assembling and validating a heart failure-free cohort from the Reasons for Geographic and Racial Differences in Stroke (REGARDS) study. BMC Medical Research Methodology **20**(1), 53 (2020) <https://doi.org/10.1186/s12874-019-0890-x> . Accessed 2024-11-01

[53] McDonagh, T.A., Metra, M., Adamo, M., Gardner, R.S., Baumbach, A., Böhm, M., Burri, H., Butler, J., Čelutkienė, J., Chioncel, O., Cleland, J.G.F., Coats, A.J.S., Crespo-Leiro, M.G., Farmakis, D., Gilard, M., Heymans, S., Hoes, A.W., Jaarsma, T., Jankowska, E.A., Lainscak, M., Lam, C.S.P., Lyon, A.R., McMurray, J.J.V., Mebazaa, A., Mindham, R., Muneretto, C., Francesco Piepoli, M., Price, S., Rosano, G.M.C., Ruschitzka, F., Kathrine Skibeland, A., ESC Scientific Document Group: 2021 ESC Guidelines for the diagnosis and treatment of acute and chronic heart failure: Developed by the Task Force for the diagnosis and treatment of acute and chronic heart failure of the European Society of Cardiology (ESC) With the special contribution of the Heart Failure Association (HFA) of the ESC. European Heart Journal **42**(36), 3599–3726 (2021) <https://doi.org/10.1093/eurheartj/ehab368> . Accessed 2024-11-01

Appendix A Extended data

A.1 Heart failure label verification

To verify the validity of the HF label, several investigations were conducted. The primary goal was to establish the label specificity and to prevent the mislabeling of non-HF cases as positive HF diagnoses. The validity analyses were performed for all the HF diagnoses in the database, that is, before applying the “recording date before 2010 or after 2023” and “HF before recording” exclusion criteria (main Figure 2).

(1) Prescribed medication analysis: This method was considered as the most informative, following validation approaches applied in prior studies [23, 52]. Medication prescriptions were analyzed from five guideline-directed medical therapy groups recommended for HF patients [3, 53]. These groups included MRA, SGLT2i, agents targeting the renin-angiotensin system (including ACE inhibitors, ARBs, and ARNIs), diuretics (both low- and high-ceiling), and beta-blockers. The complete list of medications, along with their corresponding ATC codes, is provided in Extended Data Table A2. The proportion of patients receiving these drugs was determined based on prescription dates relative to the time of HF diagnosis.

In Extended Data Figure 2, the prescription patterns are presented by dividing patients into categories according to their prescription starting time. The categories included the entire data collection period. A “new or renewed” prescription was defined as one started during the year before and the first year after diagnosis. Renewed prescription in the period was defined as if it was used previously but not during the second year before diagnosis. A “future prescription” referred to those started after the first year following diagnosis. Finally, a “history of prescription” indicated prescriptions already given before the two years preceding diagnosis. For patients without any prescriptions recorded in the available data period, the category “not documented” was assigned.

A “minimum 1” group was included to capture whether patients had received at least one drug from the specified medication groups. This assignment was made by following a priority order, where the “new or renewed” category took precedence over “future prescription”, which in turn took precedence over “history of prescription”, followed finally by “not documented”. It was found that 71.6% of HF patients had been prescribed at least one medication group during the “new or renewed” period, and another 10.4% after this period. In addition, more than 99% were treated with at least one drug from those groups. For some patients with a new HF diagnosis, differences in pharmacological treatment included dose adjustments and changes in specific drugs within the therapeutic class. Although not explicitly detailed, these adjustments are reflected in the overall usage proportions.

(2) Repeated HF diagnosis analysis: The repeated documentation of HF diagnoses across multiple patient visits is expected to improve diagnostic specificity. It was confirmed that diagnoses were not automatically re-documented during each new visit but were recorded only when deemed relevant to the visit’s content by the physician. Since multiple visits for HF-related reasons may reflect greater disease severity, excluding patients with only a single or few documented diagnoses could introduce selection bias by disproportionately excluding those with milder forms of the disease. This exclusion could also reduce both the sensitivity of the study and the sample size available for analysis. To mitigate these concerns and to decide whether repeated HF documentations should be used as an inclusion criteria, a comparison of demographic characteristics and comorbidity prevalence was conducted among patients with one, two, and three documented HF diagnoses, as presented in Extended Data Table A3. No significant differences were identified between these groups.

(3) Echocardiogram examinations analysis: A corresponding analysis to the medication prescription evaluation was conducted for variables related to transthoracic or transesophageal echocardiogram (TTE or TEE) examinations, as shown in Extended Data Figure 3. It was expected that patients diagnosed with HF would have a documented TTE or TEE examination around the time of diagnosis. The analysis classified examinations into three categories. The “inside range” category included examinations performed from one year before to two years after the initial diagnosis. Examinations documented outside of this period were assigned to the “outside range” category, while cases with no documented examination during the available data period were classified as “not documented.” It was observed that 82.5% of HF patients had undergone at least one echocardiogram examination within the defined “inside range” period. Since the TLHE dataset excludes echocardiograms performed during hospitalization, this result aligns with expectations.

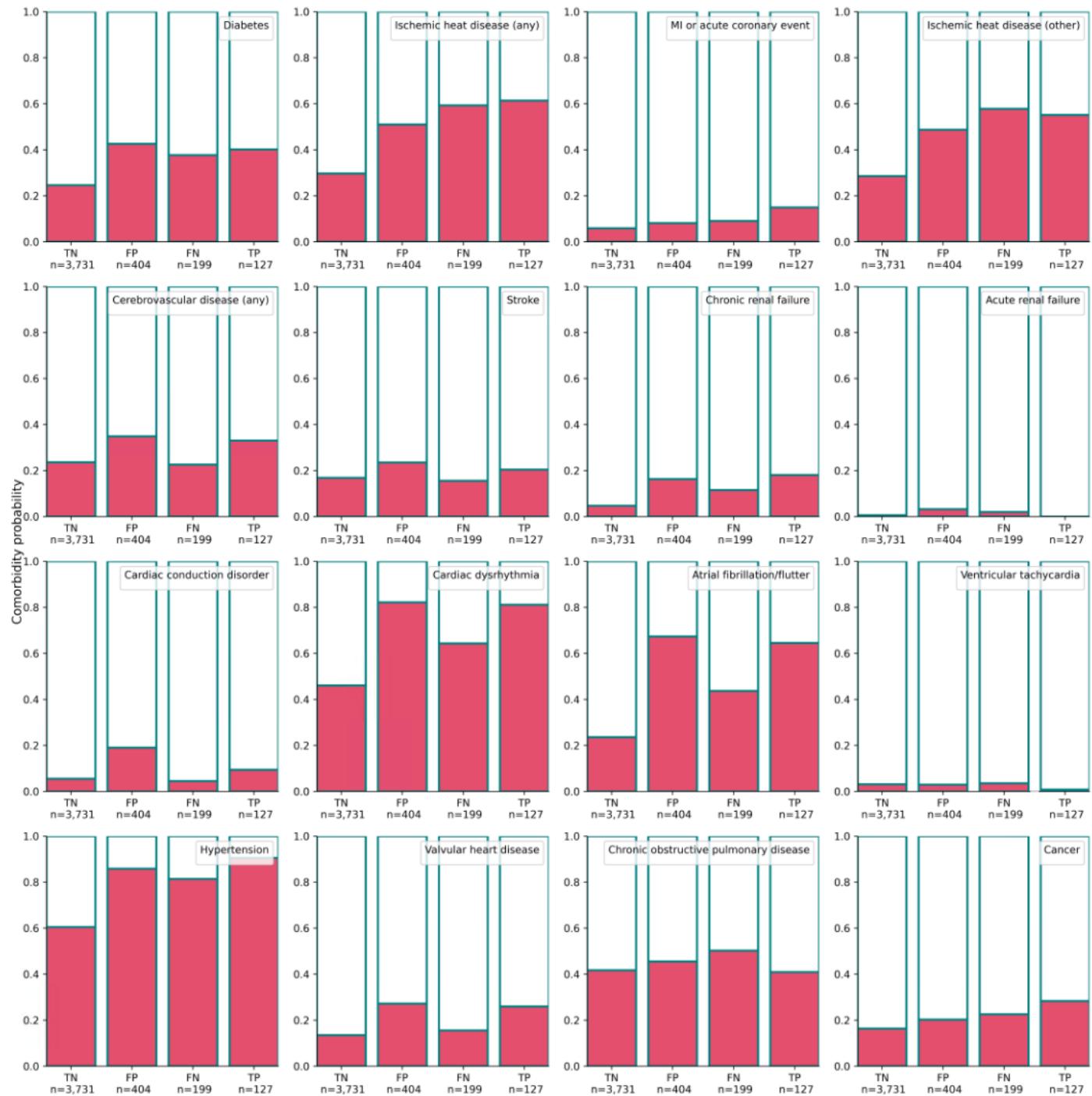
(4) Comparing between populations with/without hospital diagnosis data: Patients were additionally compared based on whether their first HF diagnosis occurred before or after 2018, the year when hospital diagnoses were incorporated into the dataset, potentially enhancing the sensitivity of the diagnostic labels. As shown in Extended Data Table A3, the different population subsets exhibited similar characteristics.

Furthermore, the analyses of prescribed medications and echocardiogram examinations were expanded to include additional groups: patients without an HF diagnosis ($\#HF = 0$), those with a low number of HF diagnoses ($0 < \#HF < 3$), and those with a high number of diagnoses ($\#HF \geq 3$), as shown in Extended Data Figure 4. “New or renewed” prescriptions for at least one medication group were identified in 58.5% and 76.4% of patients with low and high numbers of HF diagnoses, respectively. In patients of $\#HF \geq 3$, there was a higher proportion of new high-ceiling diuretic prescriptions following diagnosis with 63.5% for $\#HF \geq 3$ versus 38.2% for $0 < \#HF < 3$, with an overall usage rate of 86.6% in this group. This finding supports the hypothesis that the frequency of HF documentation correlates with disease severity and may serve as an additional indicator. Similarly, echocardiogram examinations within the “inside range” period were documented for 75.4% and 85.0% of patients with low and high numbers of HF diagnoses, respectively.

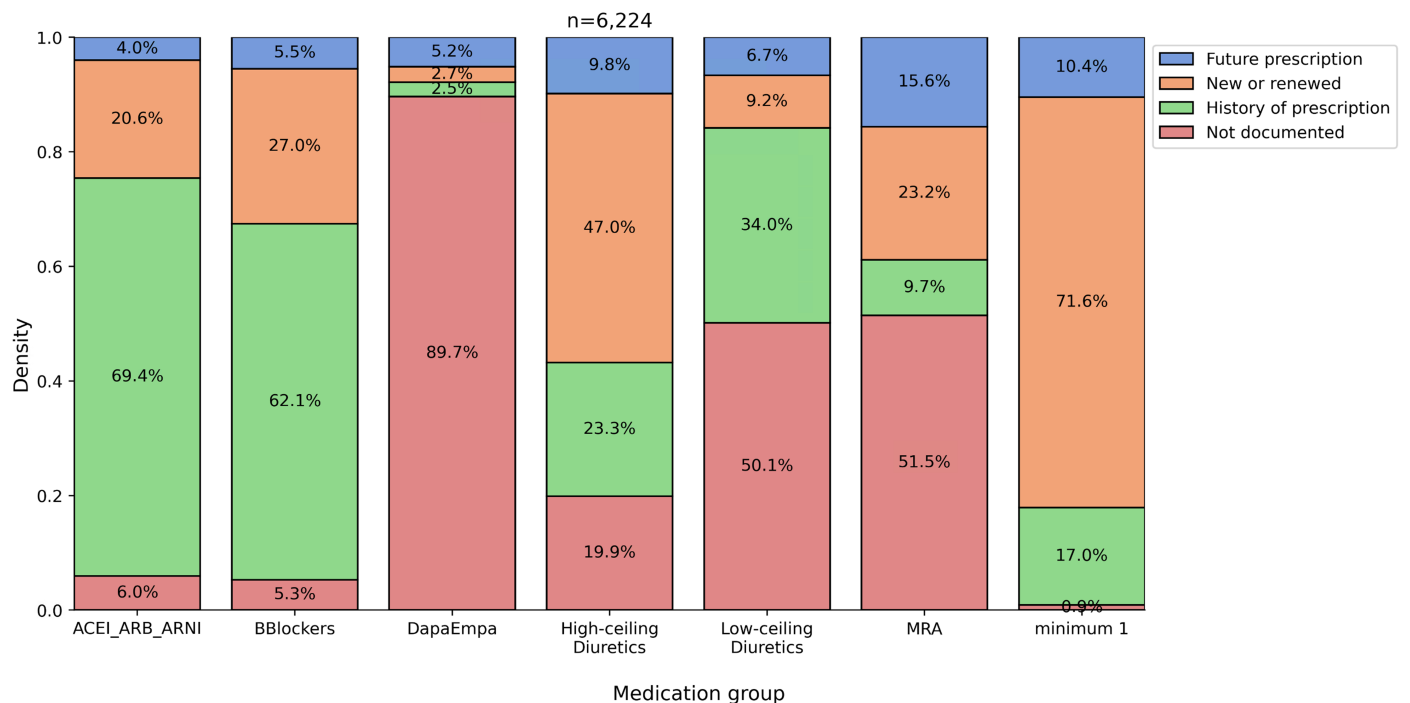
A.2 Window selection strategy for training steps

As described in Main Figure 6, in the first encoder training step, a window of 30 seconds was selected randomly from every consecutive 3 minute segment of the recording. This ended up with 480 windows of 30-second from each recording, i.e., a total of 4 hours was processed. In the second sequential step, a 30-second window was selected randomly within a 2-minute segment only once, and then the specific position inside the segment was applied for all the consecutive 2-minute segments. Thus, the gap between each 30-second window was a constant of 2 minutes. In this second step, the number of sequence elements was search as a hyper-parameter. The optimal number according to the validation set was 720, thus a total of 6 hours sampling the whole recording. This strategy allowed to reduce the computational load used. The randomization of the 30 seconds sampled made it in practice to be used as data augmentation technique, since in each epoch a different form of the same signal was used.

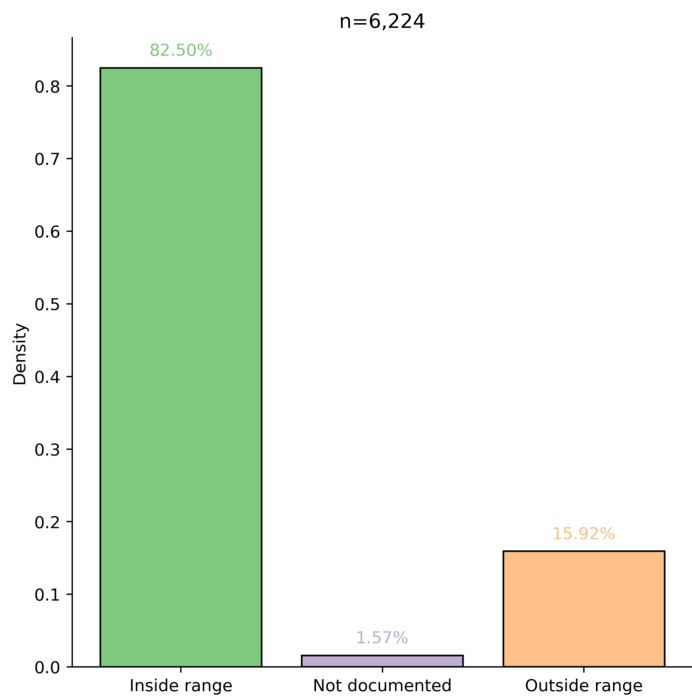
Extended data figures



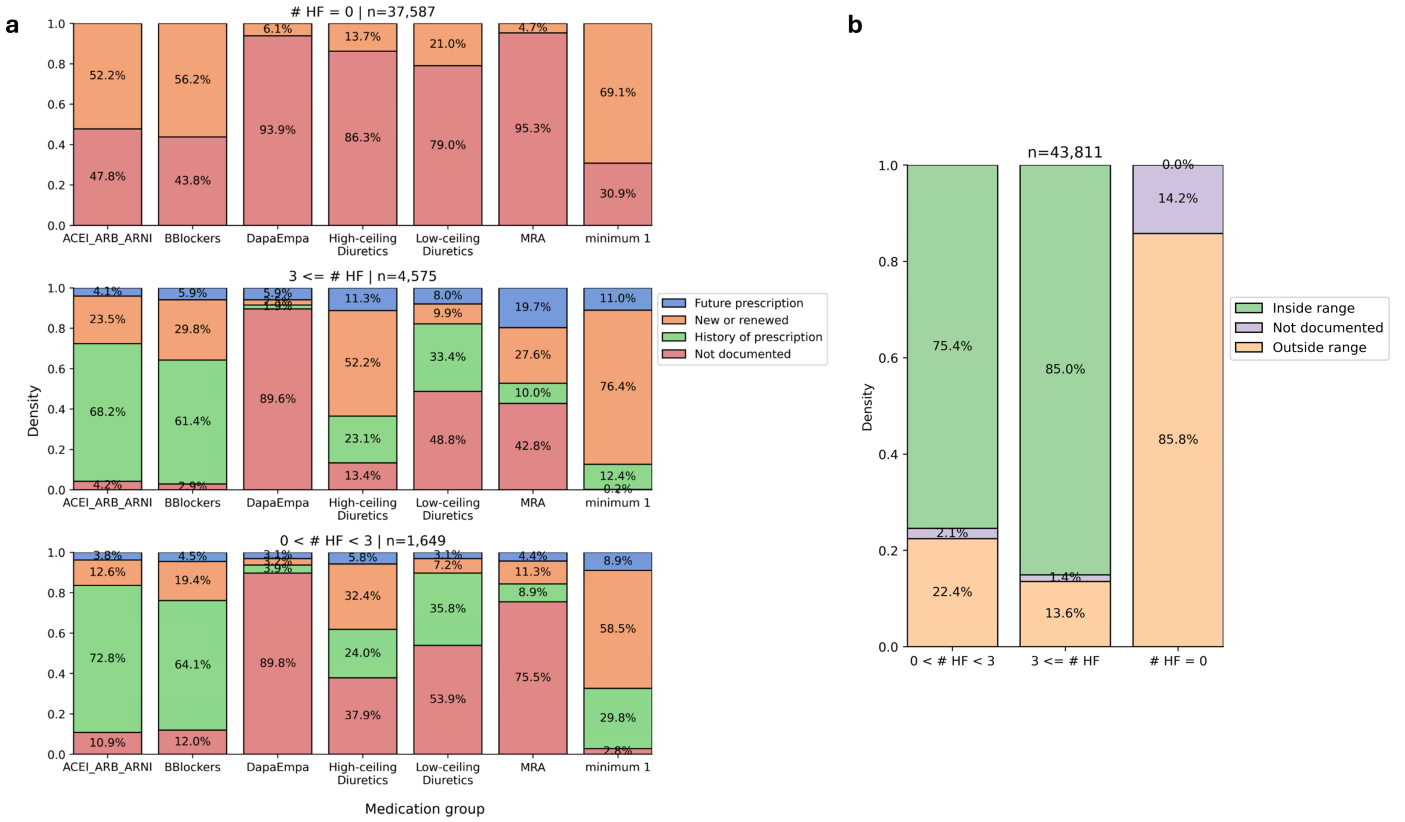
Extended Data Fig. 1: Probability of the comorbidities described in Main Table 1 divided into the classification groups. A threshold yielding a specificity of 90% was used, correspondingly to the high-risk threshold in Main Figure 3c.



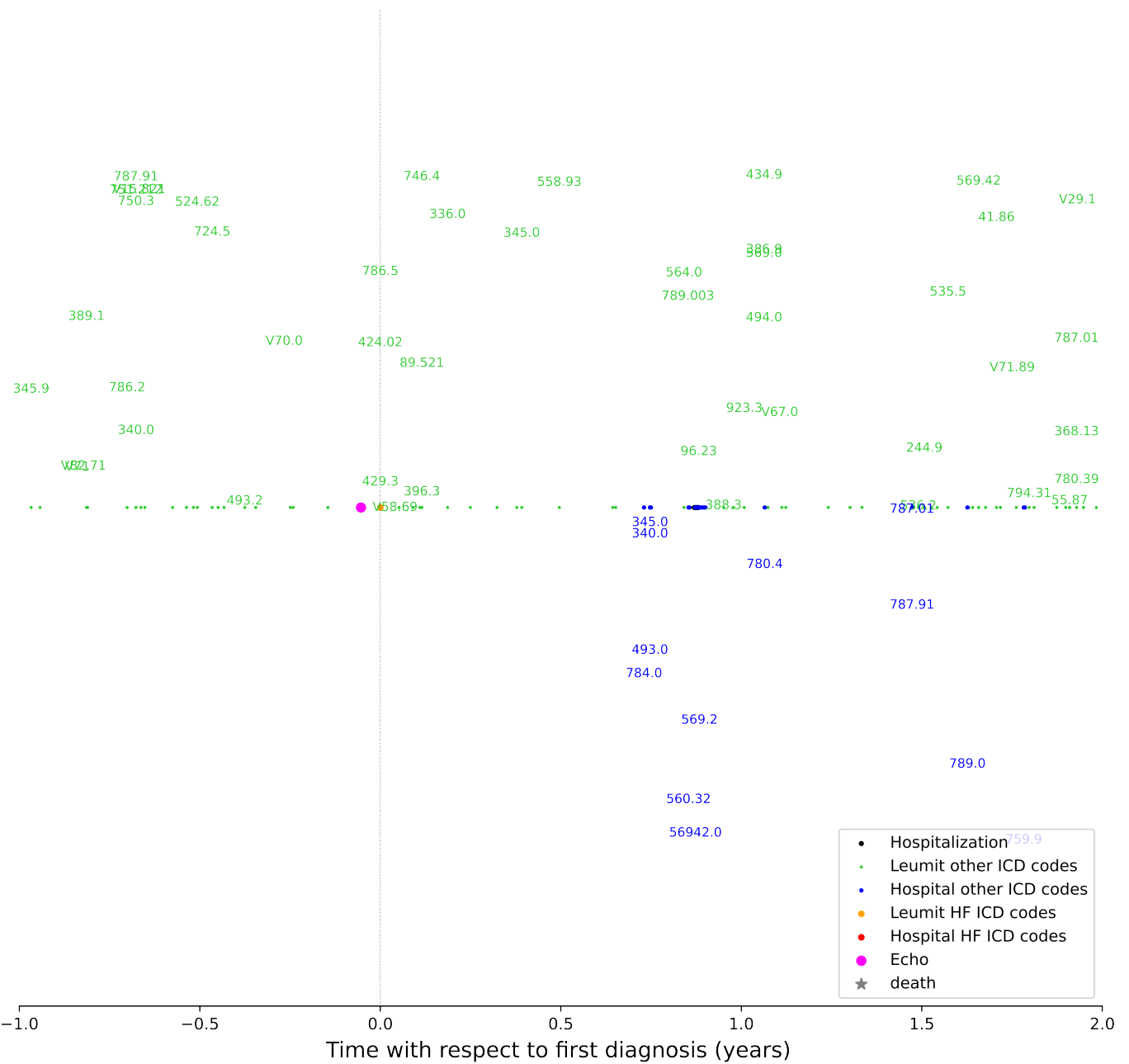
Extended Data Fig. 2: HF label verification by examining variables of prescribed medications associated with HF treatment. Comparison is between four periods with respect to interval between prescription and diagnosis. The medication groups are detailed in Extended Data Table A2: Mineralocorticoid receptor antagonists (MRA); Sodium-glucose co-transporter-2 (SGLT2) inhibitors (DapaEmpa); Angiotensin-converting enzyme inhibitors (ACE-I); Angiotensin II receptor blockers (ARB); Angiotensin receptor-neprilysin inhibitors (ARNI); Diuretics (exc. MRA); and Beta-adrenergic blocking agents (BBlockers).



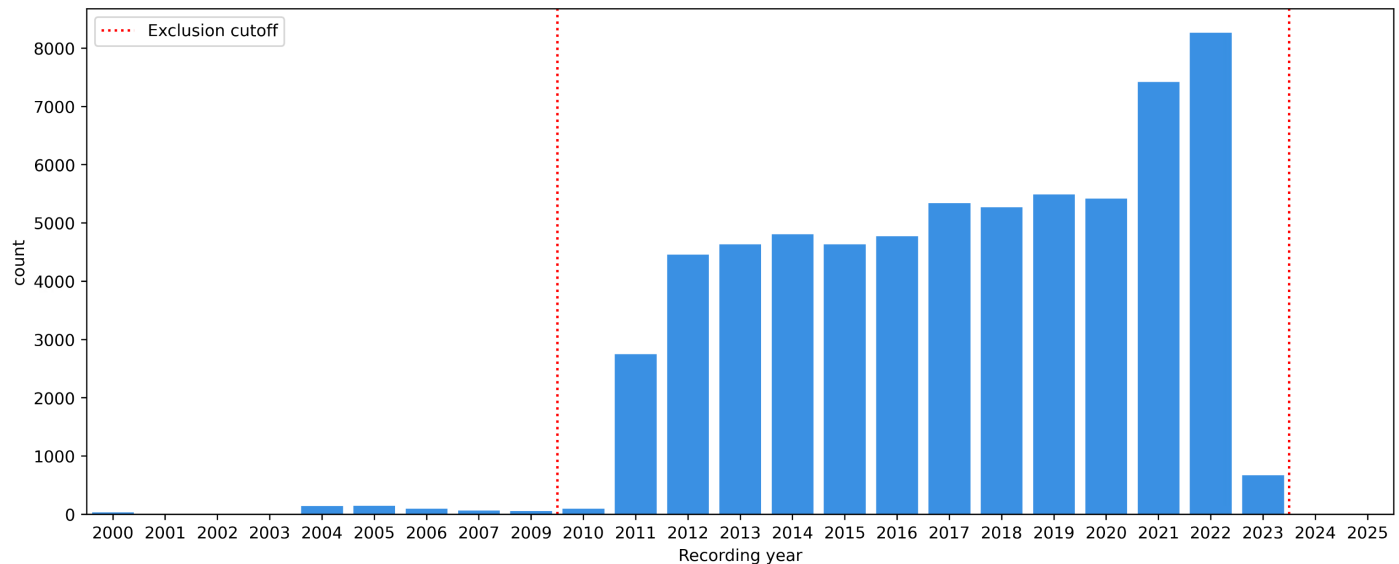
Extended Data Fig. 3: HF label verification by examining extracted variables of TTE/TEE (echocardiogram) examinations. Comparison is between three periods: during a range with respect to the first HF diagnosis (“inside range”), at any other time (“outside range”), or never (“not documented”). . Range: one year before or two years after the first diagnosis.



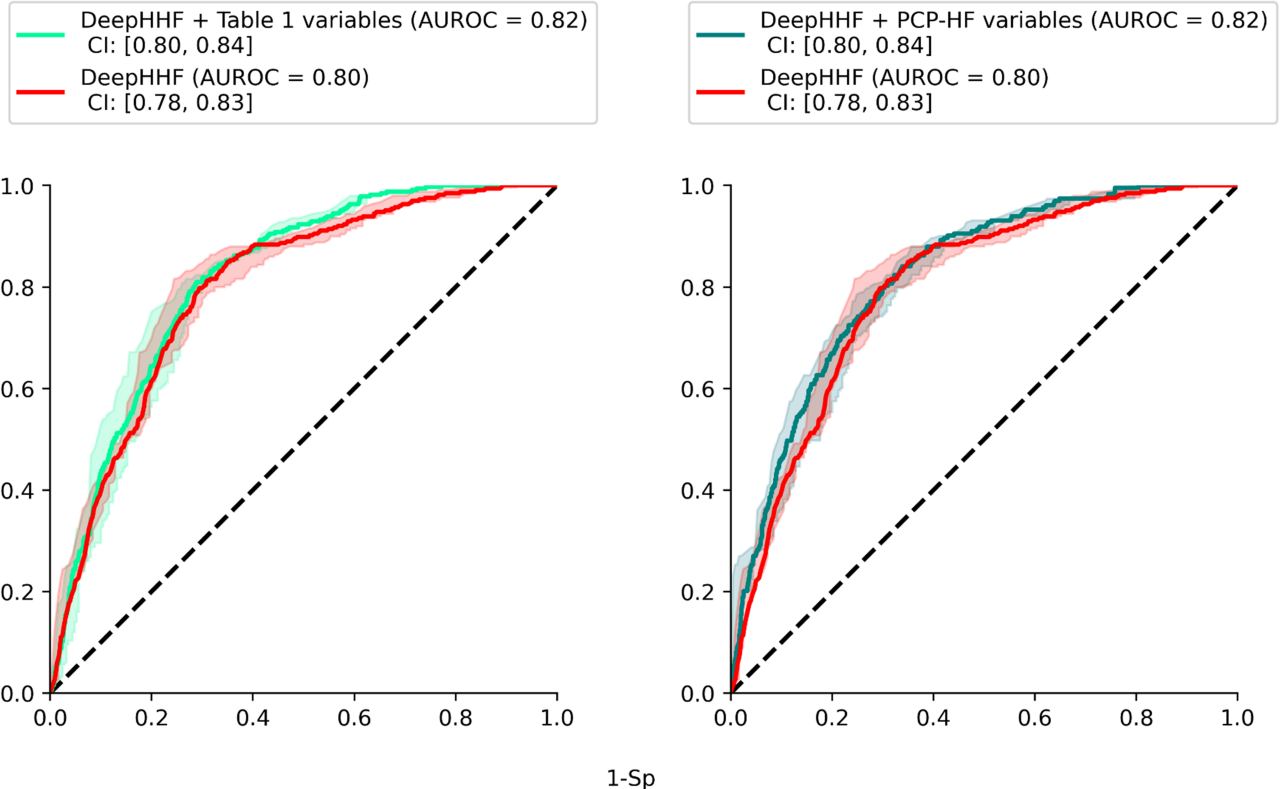
Extended Data Fig. 4: Extended analysis for HF label verification by examining variables associated with HF treatment and the repeated entries of HF diagnoses in the EMR. Comparison is between the $HF \geq 3$, $0 < HF < 3$, and $HF = 0$ (non-HF population). **a**, Extension for Extended Data Figure 2. **b**, Extension for Extended Data Figure 3.



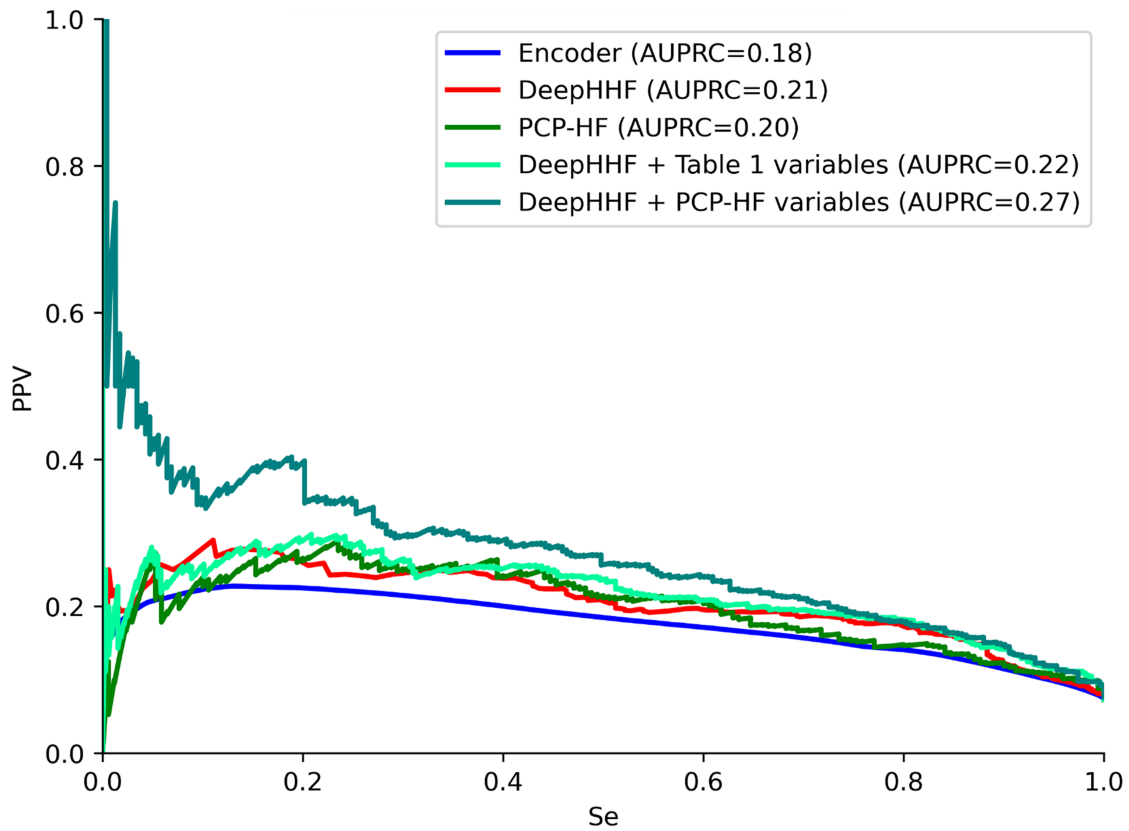
Extended Data Fig. 5: Example of an individual analysis for an outlier patient case with a positive HF diagnosis. The figure illustrates the detailed validation approach used to review the patient's medical records around their first HF occurrence. This visualization includes the full set of ICD-9 codes recorded for the patient both in hospital and in primary care (Leumit), alongside other relevant events such as echocardiography examinations, hospitalizations, or death. In this case, the echocardiography performed shortly before the HF event strengthened the confidence in the HF diagnosis.



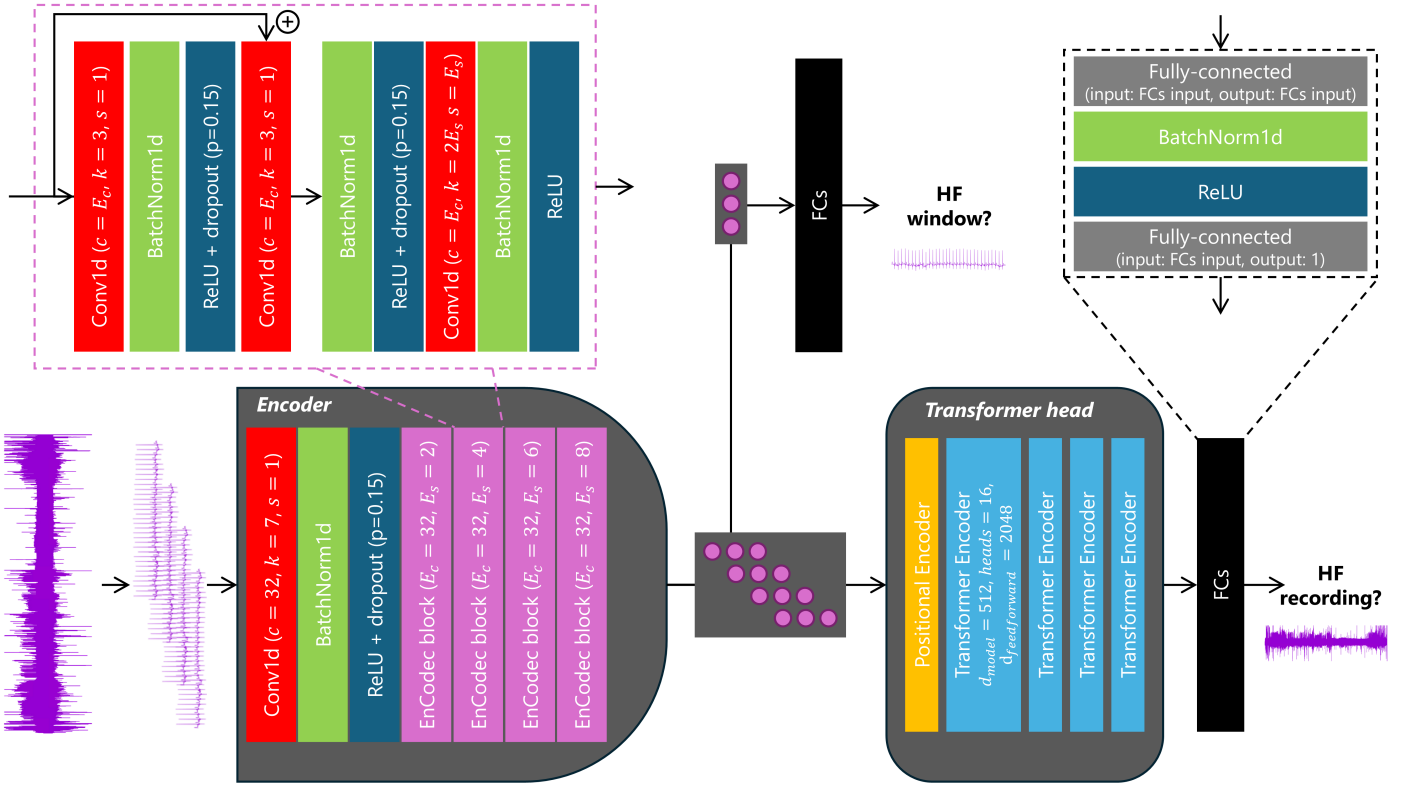
Extended Data Fig. 6: Histogram of the Holter recordings dates. Holter recordings with inconsistent timestamps were considered outliers or misdated and were therefore excluded. Systematic recording began in 2010, with the last recording collected in 2023. Consequently, the data inclusion interval for the study cohort spans from 2010 to 2023, as marked by the red dotted lines.



Extended Data Fig. 7: Combining variables with the DeepHHF score. A logistic regression classifier was trained to combine the variables together with the DeepHHF score. Receiver operating characteristic curves (ROC) were produced for the test set. The area under ROC (AUROC) scores are provided with 95% confidence intervals (CI), shown as shaded area and evaluated by bootstrapping the test set. **a**, DeepHHF taking as input the 24-hour single ECG recording (red) vs. combining the demographic and comorbidity history features listed in Table 1 to the DeepHHF score (light green). **b**, DeepHHF vs. combining PCP-HF features to the DeepHHF score (teal).



Extended Data Fig. 8: Precision-recall curves for the different reported models. The curves of positive predictive value (PPV) versus sensitivity (Se), together with their area under precision-recall curve (AUPRC) scores, are reported for the models shown in Figure 3 and Extended Data Figure 7.



Extended Data Fig. 9: Model architecture. The full 24-hour recording is split to 30-second windows, then going into the encoder, which outputs features for each window. The encoder includes EnCodec blocks, adopted from Défossez et al [44] (purple frame). These blocks are changing according to their parameters E_c (number of convolution filters) and E_s (convolution stride). Next, in the first training step, each window features are going into fully-connected layers (FCs) block (black frame) for window heart failure (HF) prediction. In the second training step, all windows are used together as input to the transformer head, added with positional encoding, and through three transformer encoders. For the final prediction of the recording, the output of the transformer head is going through a different set of FCs.

Extended data tables

Table A1: International Classification of Diseases - Ninth Revision (ICD-9) codes used for the HF end point and comorbidities.

#	Diagnosis		ICD-9 codes
End point:			
1	Heart failure (HF)		428.X, 402.01X, 402.11X, 402.91X, 404.01X, 404.03X, 404.11X, 404.13, 404.93X, 416.11X, 514.2X, 514.3X, 518.4X
Comorbidities:			
2	Diabetes		249-250.X
3	Ischemic heart disease	Any	410-414.X
4		MI or acute coronary event	410-412.X
5		Other	413-414.X
6	Cerebrovascular disease	Any	430-438.X
7		Stroke	431.X, 433.X1, 434.X1, 435.X, 436.X, 438.X
8	Chronic renal failure		585.6X, 586.X
9	Acute renal failure		584.X
10	Cardiac conduction disorders		426.X
11	Cardiac dysrhythmias	Any	427.X
12		Atrial fibrillation or flutter	427.3X
13	Hypertension		401-405.X
14	Valvular heart disease		394.X, 385.X, 397.X, 398.X, 424.X
15	Chronic obstructive pulmonary disease		490-496.X
16	Cancer		140-159.9X, 160-165.9X, 170-176.9X, 179-189.9X, 190-199.2X, 200-208.92X, 209-209.79X

Table A2: Medication group for heart failure label verification and their anatomical therapeutic chemical (ATC) classification codes.

#	Heart failure guideline-directed medical therapies groups	Included ATC codes
1	MRA ¹	ATC5Cd= 'C03DA' ATC7Cd= 'C03DA01' , 'C03DA04'
2	SGLT2i (DapaEmpa) ²	ATC7Cd= 'A10BD20' A10BD15'
3	Agents acting on the renin-angiotensin system (ACE-I, ARB, ARNI) ³	ATC3Cd= 'C09'
4	Low-ceiling Diuretics	ATC4Cd= 'C03A', 'C03B'
5	High-ceiling Diuretics	ATC4Cd= 'C03C'
6	Beta-blockers (Bblockers) ⁴	ATC3Cd= 'C07'

¹ Mineralo-corticoid receptor antagonists.

² Sodium-glucose cotransporter 2 inhibitors (including Dapagliflozin and Empagliflozin).

³ Agents acting on the renin-angiotensin system (including angiotensin-converting enzyme inhibitors (ACE-I), angiotensin receptor blockers (ARB), angiotensin receptor-neprilysin inhibitors (ARNI)).

⁴ Beta-adrenergic blocking agents.

Table A3: Comparison between patients with different # of first heart failure (HF) diagnosis repeated in their files. The table concentrates on the cases of 1, 2 and 3 repeated diagnoses. The table separates between diagnosis given before and after 2018, since after 2018 the data included diagnosis registered in hospitals as well.

		First HF diagnosis after 2018			First HF diagnosis before 2018			
		1	2	3	1	2	3	
Diagnosis age	18-39	11 (2.0%)	2 (0.43%)	2 (0.83%)	5 (1.47%)	4 (1.37%)	2 (1.2%)	
	40-49	26 (4.74%)	14 (2.99%)	6 (2.49%)	10 (2.95%)	6 (2.06%)	8 (4.79%)	
	50-59	55 (10.02%)	34 (7.25%)	23 (9.54%)	19 (5.6%)	18 (6.19%)	11 (6.59%)	
	60-69	154 (28.05%)	112 (23.88%)	54 (22.41%)	71 (20.94%)	65 (22.34%)	32 (19.16%)	
	70-79	178 (32.42%)	187 (39.87%)	90 (37.34%)	112 (33.04%)	93 (31.96%)	63 (37.72%)	
	80+	125 (22.77%)	120 (25.59%)	66 (27.39%)	122 (35.99%)	105 (36.08%)	51 (30.54%)	
Sex	F	286 (52.09%)	259 (55.22%)	121 (50.21%)	195 (57.35%)	156 (53.61%)	74 (44.31%)	
	M	263 (47.91%)	210 (44.78%)	120 (49.79%)	145 (42.65%)	135 (46.39%)	93 (55.69%)	
BMI	0-18.5	7 (1.3%)	3 (0.66%)	1 (0.43%)	4 (1.51%)	2 (0.82%)	0 (0.0%)	
	18.5-25	93 (17.25%)	76 (16.78%)	47 (20.0%)	44 (16.6%)	54 (22.04%)	34 (24.46%)	
	25-30	187 (34.69%)	185 (40.84%)	96 (40.85%)	111 (41.89%)	101 (41.22%)	52 (37.41%)	
	30-35	165 (30.61%)	112 (24.72%)	57 (24.26%)	57 (21.51%)	59 (24.08%)	31 (22.3%)	
	35-40	51 (9.46%)	47 (10.38%)	25 (10.64%)	29 (10.94%)	18 (7.35%)	19 (13.67%)	
	40+	36 (6.68%)	30 (6.62%)	9 (3.83%)	20 (7.55%)	11 (4.49%)	3 (2.16%)	
Smoking	Not smoking	467 (85.06%)	397 (84.65%)	207 (85.89%)	290 (85.29%)	248 (85.22%)	140 (83.83%)	
	Previously/currently	77 (14.03%)	66 (14.07%)	31 (12.86%)	27 (7.94%)	31 (10.65%)	19 (11.38%)	
	Unknown	5 (0.91%)	6 (1.28%)	3 (1.24%)	23 (6.76%)	12 (4.12%)	8 (4.79%)	
Comorbidities	Diabetes	236 (42.99%)	223 (47.55%)	114 (47.3%)	156 (45.88%)	131 (45.02%)	77 (46.11%)	
	Ischemic heart disease	Any	253 (46.08%)	258 (55.01%)	145 (60.17%)	193 (56.76%)	180 (61.86%)	111 (66.47%)
		MI or acute coronary event	86 (15.66%)	92 (19.62%)	45 (18.67%)	69 (20.29%)	56 (19.24%)	44 (26.35%)
	Cerebrovascular disease	Other	238 (43.35%)	244 (52.03%)	139 (57.68%)	185 (54.41%)	172 (59.11%)	105 (62.87%)
		Any	154 (28.05%)	161 (34.33%)	89 (36.93%)	131 (38.53%)	120 (41.24%)	68 (40.72%)
	Stroke	Stroke	118 (21.49%)	125 (26.65%)	66 (27.39%)	99 (29.12%)	89 (30.58%)	54 (32.34%)
		Chronic renal failure	67 (12.2%)	72 (15.35%)	32 (13.28%)	49 (14.41%)	57 (19.59%)	33 (19.76%)
	Cardiac dysrhythmia	Acute renal failure	11 (2.0%)	11 (2.35%)	7 (2.9%)	6 (1.76%)	4 (1.37%)	3 (1.8%)
		Cardiac conduction disorder	44 (8.01%)	33 (7.04%)	22 (9.13%)	29 (8.53%)	34 (11.68%)	18 (10.78%)
	Hypertension	Any	198 (36.07%)	218 (46.48%)	121 (50.21%)	168 (49.41%)	153 (52.58%)	75 (44.91%)
		Atrial fibrillation/flutter	121 (22.04%)	141 (30.06%)	83 (34.44%)	106 (31.18%)	98 (33.68%)	52 (31.14%)
		Ventricular tachycardia	8 (1.46%)	10 (2.13%)	7 (2.9%)	4 (1.18%)	5 (1.72%)	3 (1.8%)
	Valvular heart disease	Valvular heart disease	77 (14.03%)	88 (18.76%)	49 (20.33%)	76 (22.35%)	86 (29.55%)	36 (21.56%)
		Chronic obstructive pulmonary disease	248 (45.17%)	211 (44.99%)	126 (52.28%)	173 (50.88%)	146 (50.17%)	71 (42.51%)
		Cancer	105 (19.13%)	109 (23.24%)	60 (24.9%)	72 (21.18%)	64 (21.99%)	46 (27.54%)